AD-A104 039   MASSACHUSETTS INST OF TECH CAMBRIDGE DEPT OF CHEMISTRY   F/G 7/4
   LOWEST ENERGY ELECTRONIC STATES OF RARE EARTH MONOXIDES.(U)
                SEP 80   R W FIELD   F19628-77-C-0061
UNCLASSIFIED   AFGL-TR-80-0328   NL

AFGL-TR-80-0328

LOWEST ENERGY ELECTRONIC STATES OF
RARE EARTH MONOXIDES

Robert W. Field

Massachusetts Institute of Technology
Department of Chemistry
Cambridge, Massachusetts 02139

Final Report
1 January 1977 - 15 August 1980

1 September 1980

SEP 10 1981

81 9 10 037

(19) REPORT DOCUMENTATION PAGE		READ INSTRUCTIONS BEFORE COMPLETING FORM
1. REPORT NUMBER AFGL-TR-80-0328	2. GOVT ACCESSION NO. AD A104039	3. RECIPIENT'S CATALOG NUMBER
4. TITLE (and Subtitle) Lowest Energy Electronic States of Rare Earth Monoxides		5. TYPE OF REPORT & PERIOD COVERED Final Scientific 1 Jan 1977-15 Aug 1980
		6. PERFORMING ORG. REPORT NUMBER
7. AUTHOR(s) Robert W. Field		8. CONTRACT OR GRANT NUMBER(s) F 19628-77-C-0061
9. PERFORMING ORGANIZATION NAME AND ADDRESS Department of Chemistry Massachusetts Institute of Technology Cambridge, Massachusetts 02139		10. PROGRAM ELEMENT, PROJECT, TASK AREA & WORK UNIT NUMBERS 61102F 2303G1AA
11. CONTROLLING OFFICE NAME AND ADDRESS Air Force Geophysics Laboratory (LKB) Hanscom Air Force Base, Mass. 01731 Monitor/Edmond Murad/LKB		12. REPORT DATE 1 September 1980
		13. NUMBER OF PAGES 102
14. MONITORING AGENCY NAME & ADDRESS(If different from Controlling Office) Office of Naval Research Massachusetts Institute of Technology		15. SECURITY CLASS. (of this report) Unclassified
		15a. DECLASSIFICATION/DOWNGRADING SCHEDULE

16. DISTRIBUTION STATEMENT (of this Report)

Approved for public release; distribution unlimited.

17. DISTRIBUTION STATEMENT (of the abstract entered in Block 20, if different from Report)

18. SUPPLEMENTARY NOTES

19. KEY WORDS (Continue on reverse side if necessary and identify by block number)

Thermochemistry, Rare Earth Monoxides, Diatomic Molecules, Laser Spectroscopy, Tunable Lasers, Fluorescence, Flame Species

20. ABSTRACT (Continue on reverse side if necessary and identify by block number)

Extensive studies of the electronic structure of CeO and PrO have been completed. More than 15 electronic states for both molecules, lying below 5000 cm^{-1} have been identified. A crystal field model for the electronic structure of CeO has been developed and tested. Exploratory studies of the electronic structures of EuO, YbO, and CuO have been initiated. This research program has led to publication of 5 papers, with 5 more in preparation.

DD $_{1 JAN 73}^{FORM}$ 1473 EDITION OF 1 NOV 65 IS OBSOLETE
S/N 0102-LF-014-6601

BLANK PAGE

LOWEST ENERGY ELECTRONIC STATES OF THE RARE EARTH MONOXIDES

A. INTRODUCTION

The electronic spectra of the rare earth monoxides have been nearly intractable for two reasons: There is a tremendous number of molecular electronic states (typically more than 100) expected to occur below 3eV, these states all have nearly identical rotational and vibrational constants (to within 2%) and are, therefore, not readily distinguishable from each other. It has been necessary to develop laser spectroscopic methods which are capable of resolving and dealing unambiguously with complex spectra, recognizing individual electronic states and organizing them into partial energy level diagrams, and linking partial level diagrams for groups of states which, because of selection-rule restrictions, involve mostly disjoint groups of electronic states. In order to provide information of value to either thermochemists or theoreticians, it is important to know that all of the lowest energy electronic states have been found. To this end, a crystal field model, which relates the molecular energy levels to those of the free M^{+2} ion, has been developed and tested for the 4f6s configuration of CeO.

A number of publications have resulted from this contract and these are attached to this report as Appendix. Briefly, the results are summarized below.

B. SUMMARY OF RESULTS

1. CeO Electronic Structure

In collaboration with Professor C. Linton (University of New Brunswick, CANADA), Dr. R.F. Barrow (Oxford University, ENGLAND), and Dr. P. Carette (Université des Sciences et Techniques de Lille, FRANCE), an energy level diagram for CeO has been constructed which incorporates all known electronic transitions. Below 4500 cm^{-1}, there are expected to be 16 molecular states derived from the $Ce^{+2}(4f6s)O^{-2}(^1S)$ configuration, of which we have located 15. The energies of these states are well represented by a 5-parameter crystal field model, which should also be applicable to higher lying states of CeO as well as to other rare earth monoxides and monohalides. Several hidden Hund's case 'c' quantum numbers have been revealed by this model; these include the M^{+2} total angular momentum, J_a, and parity.

2. PrO Electronic Structure

The lowest energy configuration for PrO is probably $Pr^{+2}(4f^2 6s)$ which gives rise to 91 Ω-doubled molecular electronic states (within a 30,000 cm^{-1} energy range). Other low-lying configurations ($f^2 d \rightarrow 910$, $f^3 \rightarrow 364$) give rise to far more states. An important clue to the configurational parentage of each electronic state of PrO, which is not available for the $I = 0$ $^{140}Ce_{58}$ monoxide, is the $^{141}Pr_{59}$ $I = 5/2$ magnetic hyperfine structure. The rotational and hyperfine structure of PrO electronic

systems XII through XXII has been analyzed. Fluorescence spectra excited via assigned lines from the above systems reveal numerous (>11) low-lying electronic states and have permitted construction of several partial energy level diagrams. All but one of the states for which hyperfine structure is observed derive from configurations involving a singly occupied Pr^{+2} 6s orbital. We expect to be able to make configurational and J_a assignments for the $4f^2 6s$ states of PrO and to predict the approximate energies (to ± 500 cm^{-1}) of all 91 states of this configuration.

3. EuO, YbO, and CuO

The excitation and fluorescence spectra of the 599 nm band of EuO have been recorded. Exploratory spectra of YbO have been recorded. Doppler-limited excitation spectra of the CuO $A^2\Sigma-X^2\Pi$ and $A'^2\Sigma-X^2\Pi$ systems reveal hyperfine structure only the the latter system, which will be useful in determining the configurational parentage of the X, A, and A' states.

4. PUBLICATIONS

The publications which have resulted from this work are:

1. C. Linton, M. Dulick and R.W. Field, "Laser Spectroscopy of CeO. Fluorescence of the C_1-X_1 and D_3-X_3 Systems," J. Mol. Spectrosc. 78, 428-436 (1979).

2. M. Dulick, R.W. Field and J. Cl. Beaufils, "On the Hyperfine Structure of the 0-0 Band in the PrO XVII System," J. Mol. Spectrosc. 78, 333-334 (1979).

3. C. Linton, P. Carette, R.W. Field, M. Dulick and R.F. Barrow, "Low Lying States of CeO," J. Chem. Phys. 74, 189-191 (1981).

4. O. Appelblad, A. Lagerqvist, I. Renhorn, and R.W. Field, "The Spectrum of CuO: Low Lying Electronic States Observed by Laser Induced Fluorescence," Physica Scripta, 22, 603-608 (1980).

5. M. Dulick, R.W. Field and J. Cl. Beaufils, "Rotational and Hyperfine Analysis of the 0-0 Band of the PrO XX System," J. Mol. Spectrosc. 00, 000-000 (1981).

6. M. Dulick, R.W. Field, J. Cl. Beaufils and J. Schamps, "The Electronic Spectrum of PrO. Energy Linkages, Rotational Analysis, and Hyperfine Structure for Systems XVII and XXI," J. Mol. Spectrosc. 00, 000-000 (1981).

7. C. Linton and M. Dulick, "Optical-Optical Double Resonance Spectra of Cerium Oxide," J. Mol. Spectrosc. 00, 000-000 (1981).

8. C. Linton, M. Dulick, and R.W. Field, "Laser Spectroscopy of CeO: Identification and Assignment of the Low Lying States," J. Mol. Spectrosc. 00, 000-000 (1982).

5. <u>INTERACTIONS AND PRESENTATIONS</u>

4-79 Air Force Geophysics Laboratory, Hanscom AFB, "What You Wanted to Know About Spectroscopic Properties of Small Molecules But Were Afraid to Ask."

9-79 Sixth Colloquium on High Resolution Molecular Spectroscopy, Tours, FRANCE, Talks B10, J12.

J. Cl. Beaufils, P. Carette, M. Dulick and R.W. Field,

"Structure Hyperfine du Monoxyde de Praseodyme."

P. Carette, J.Cl. Beaufils, M. Dulick, and R.W. Field,

"Laser Spectroscopy of Cerium Monoxide."

6-80 Molecular Spectroscopy Symposium, Columbus, Ohio,

papers MF9, MF10.

C. Linton, M. Dulick, R.W. Field and P. Carette, "Laser

Spectroscopy of CeO: The X_2 State Manifold."

M. Dulick and R.W. Field, "The Electronic Structure

of PrO."

6. PERSONNEL

   1. Visiting Scientists

      Dr. Richard F. Barrow, Oxford University, U.K. (CeO)

      Dr. Jean-Claude Beaufils, Université des Sciences et Techniques

         de Lille, FRANCE. (PrO)

      Dr. Pierre Carette, Université des Sciences et Techniques

         de Lille, FRANCE. (CeO)

      Professor Colan Linton, University of New Brunswick, CANADA. (CeO)

   2. Postdoctorals

      Dr. Philip G. Cummins

      Dr. Ingemar Renhorn (EuO, SmO, PrO)

   3. Graduate Students

      Dr. Michael Dulick (CeO, PrO, EuO, YbO, Crystal Field Model)

      Ph.D. September 1981.

4. Undergraduates

    Mr. Alain Drooz (EuO, SmO, PrO)

    B.S. May 1980

    Mr. Paul S. Weiss (EuO)

    B.S. and M.S. May 1980

Appendix

Laser Spectroscopy of CeO

Fluorescence of the C_1-X_1 and D_3-X_3 Systems

C. Linton

Physics Department, University of New Brunswick, Fredericton, New Brunswick, Canada E3B 5A3

AND

M. Dulick and R. W. Field

Department of Chemistry and Spectroscopy Laboratory, Massachusetts Institute of Technology, Cambridge, Massachusetts 02139

Fluorescence spectra of the CeO molecule have been obtained using a chemi-luminescent Ce + O_2 flame and both argon and cw dye lasers. Spectra obtained with the 488.0 and 514.5-nm lines of an argon laser are shown to contain vibrational progressions of the $D_3(5)-X_3(4)$ and $C_1(3)-X_1(2)$ transitions, respectively. (In labeling the states, the letter and subscript refer to a specific electronic state or substate, and the number in parentheses is Ω.) Analysis of these spectra has led to a determination of vibrational constants for the X_1 state, and the separation of the two lowest vibrational levels in the C_1, D_3, and X_3 states. Transitions to several additional electronic states have also been observed.

INTRODUCTION

Recent assignments of several features in optical spectra of S-type stars to the CeO molecule (*1–3*) emphasize the need for a detailed understanding of this molecule. Laboratory studies have resulted in compilations of over 300 band-heads (*4, 5*) and extensive rotational analyses of about 36 absorption bands (*5–7*). No obvious vibrational patterns have emerged from bandhead data. Rotational analyses have provided rotational constants for 34 substates but because, with the exception of the $B_2(4)-X_2(3)$ transition, all analyzed bands are in $\Delta v = 0$ sequences, gas phase vibrational spacings have only been obtained for the B_2 and X_2 states. Vibrational frequencies, ω_v, have been estimated for other states using the Kratzer relation, $\omega_e^2 = 4B_e^3/D_e$. The analyzed bands fall mainly into three groups, each involving transitions to a common lower electronic state (or substate) with the result that eight low lying states have been observed and separations of many of the higher lying states are known. However, the data have so far only linked together two of the low lying states $(X_4(3)-X_2(3) = 2060$ cm$^{-1})$ and relative positions of the other low lying states are still unknown. Infra-red absorption measurements of CeO trapped in inert matrices (*8*) have yielded ground state vibrational spacings of 808 cm^{-1} in an argon matrix and 820 cm^{-1} in

neon. Many electronic absorption transitions, presumably from the ground state, were observed in a neon matrix from the near ultraviolet to the near infrared regions.

The above summary points to a need for further experiments designed to provide vibrational frequencies and electronic state separations. Vibrational progressions are very difficult to detect in the emission and absorption spectra as most of the intensity is concentrated in $\Delta v = 0$ sequences and the spectrum is so rich that other sequences are generally overlapped by $\Delta v = 0$ sequences of other electronic transitions.

An extensive program of experiments has been initiated using various laser techniques to provide a comprehensive energy level picture of the molecule, either by direct observation of new transitions or through perturbations. Because of the selectivity of excitation and the generally "clean" nature of the spectra, laser fluorescence spectroscopy provides vibrational frequencies and electronic state separations for low lying states. We have used both argon ion and tunable dye lasers to produce fluorescence and, in this paper, we report on vibrational progressions which are linked to two of the transitions assigned by Barrow *et al.* (5-7). Excitation of the $D_3(5)-X_3(4)$ transition by the Ar 488.0-nm line and of the $C_1(3)-X_1(2)$ transition by the 514.5- and 496.5-nm lines have enabled vibrational frequencies to be calculated for the four states involved.

EXPERIMENTAL METHOD

The general features of the apparatus used for producing metal oxides have been described previously (9). Cerium metal was evaporated from a resistively heated graphite crucible and the vapor, entrained in a flow of cool argon gas, was carried into a reaction chamber to react with an oxidant and produce a chemiluminescent flame. A laser beam was then directed into the flame region to produce fluorescence. N_2O, O_2, and CO_2 all produced flames and it was found that O_2 and CO_2 were the most suitable oxidants for fluorescence experiments. Only the slightest trace of oxidant was required in order to maximize the fluorescence.

Spectra were recorded photoelectrically using a 0.5-m Ebert Monochromator and calibrated using a mercury lamp. The relative accuracy of wavelength measurements was 0.025 nm. For 514.5-nm excitation, spectra were also photographed in the first order of a 3.4-m spectrograph at a reciprocal dispersion of 0.5 nm/mm. With a slit width of 50 μm, an exposure of 8 hr gave a measurable, though rather faint spectrum on Kodak 103 a-F plates. An iron hollow–cathode lamp was used for wavelength calibration and the relative accuracy of the measurements was 0.005 nm.

RESULTS AND ANALYSIS

Chemiluminescence spectra were obtained with both N_2O and O_2. N_2O produced a strong whitish blue flame whose spectrum, extending from the near ultraviolet to the infrared, consisted of many bands superimposed on a strong continuous background. The flame from the Ce + O_2 reaction was green and less intense than the N_2O flame. However, there was very little background, and the bands stood out much more clearly than with N_2O. The spectrum, which

430   LINTON, DULICK, AND FIELD

was very extensive and complex, was confirmed as CeO by comparison with published band lists (4, 5). Several unlisted bands appeared in the spectra and several listed bands were not observed but, on the whole, the chemiluminescence spectra matched the published lists very well. Although no new information was gained from these spectra, they did confirm that CeO was being formed by the chemiluminescent reaction.

Fluorescence was excited by each argon laser line and at several wavelengths in the dye laser (Rhodamine 6G) region. Most lines simultaneously excited several transitions and the spectra, which were fairly complex, showed the following general features.

(i) Groups of doublets (P,R) or triplets (P,Q,R) with the groups separated by 800–850 cm^{-1}. These are vibrational progressions in the lower state.

(ii) Other doublets or triplets with the same P, R (or P, Q, R) separations as the above progressions but distributed, seemingly at random, throughout the spectrum. These are probably either $\Delta v = 0$ transitions or perturbation allowed bands belonging to normally weak or forbidden transitions from the same upper level responsible for the type (i) features.

(iii) Isolated doublets or triplets, no member of which coincides with the laser frequency, and having significantly different P, R separations from the above groups. In these cases, the laser excites a very weak transition and emission is observed in more strongly allowed transitions to different vibrational or electronic states.
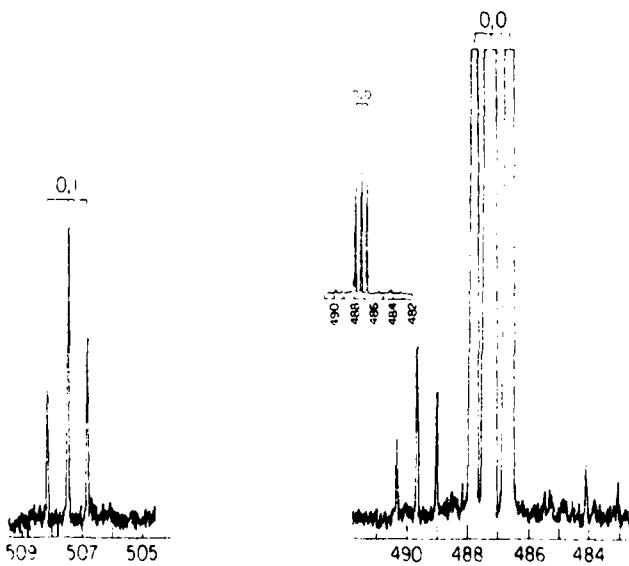

FIG. 1. Portions of the fluorescence spectrum of CeO excited by the Ar$^+$ 488.0-nm laser line at a pressure of 1 Torr. Wavelengths are in nanometers and the labeled lines belong to the $D_1(5)$–$X_3(4)$ system.

Of the many vibrational progressions observed, several did not seem to belong to transitions assigned by Barrow et al. (5–7). So far, we have analyzed progressions involving two known transitions (D_3-X_3, C_1-X_1) and the results are outlined below.

The $D_3(5)-X_3(4)$ System

Portions of the spectrum excited by the Ar$^+$ line at 488.0 nm are shown in Fig. 1. The overall spectrum was complex, but when the laser was operated single mode with the etalon adjusted to maximize the intensity of one of the intense lines, the spectrum was considerably simplified. The main features of the spectrum were an intense PQR triplet around the laser wavelength and a similar, much weaker, group of lines about 820 cm^{-1} to the red of this. These were two members of a vibrational progression. The laser excited a P branch line and, as the intensity of the group of lines near the laser frequency was about 50 times that of the other group, the excitation transition was in the $\Delta v = 0$ sequence. The absence of any equivalent triplet at shorter wavelengths suggests that the 0–0 band was excited with subsequent emission of the 0–0 and 0–1 bands. The intensity of the R line was greater than that of the P line suggesting that the transition involved $\Delta\Omega = +1$ where $\Delta\Omega = \Omega' - \Omega''$. (As $\Delta\Omega = \pm 1$ rotation–electronic perturbations can systematically alter R/P intensity ratios, independent confirmation of $\Delta\Omega = +1$ vs -1 assignments is desirable.) A similar triplet around 490 nm has not been assigned but probably involves a different lower electronic state. The measured wavelengths and frequencies are listed in Table I.

Reduction of data by standard methods, assuming that $B'' \sim 0.35$ cm^{-1}, which is typical of all analyzed states (5), showed that the laser excited $J' = 36$. The excitation was thus assigned as a $P(37)$ line. The observed R, Q, and P line

TABLE I

Photoelectric Measurements of $D_3(5)-X_3(4)$ Fluorescence Lines Excited by the Ar$^+$ 488.0-nm Line

Wavelength (nm)*	Wavenumber (cm^{-1}) Observed	Ref. 7	Assignment
486.77	20 537.8	20 538.2	R(35) 0,0
487.38	20 512.1	20 512.8	Q(36) 0,0
487.99	20 486.5	20 486.7	P(37) 0,0
507.03	19 717.2		R(35) 0,1
507.6к	19 697.0		Q(36) 0,1
508.35	19 666.0		P(37) 0,1
		20 501.1	R(35) 1,1
		20 475.8	Q(36) 1,1
		20 449.8	P(37) 1,1

*Relative accuracy 0.025 nm, 1.0 cm^{-1}

432   LINTON, DULICK, AND FIELD

frequencies were in 0.5 cm^{-1} agreement with the listed (7) $R(35)$, $Q(36)$, and
$P(37)$ lines of the $C_3(5)-X_3(4)$ 0-0 band.

The vibrational spacing in the X_3 state was calculated from

$$\Delta\nu(v,J) = \Delta G''_{r,1/2} - \alpha''_e J(J + 1) \qquad (1)$$

where $\Delta\nu(v,J)$ is the measured separation between successive P, Q, or R lines
(v'',J) and $(v'' + 1, J)$. As the 1-1 band of this transition has also been analyzed
(5, 7), α_e is known for both states, and the equivalent P, Q, and R lines of the 1-1
band (Table I) were used to calculate the vibrational spacing in the D_3 state.
As our measurements were systematically ~0.5 cm^{-1} lower than the high resolu-
tion data (7), they were increased by this amount for calculation of the spacing
in the D_3 state. The obtained values of $\Delta G_{1/2}$ are listed in Table IV.

The spectrum in Fig. 1 also shows two weak lines slightly to the red of the laser
line. This seems to be a PQR triplet with the laser exciting the $R(9)$ line and appears
to belong to the 1-1 band of the D_3-X_3 transition, an assignment which is
confirmed by high resolution data (7). No other $v' = 1$ bands were observed.

The C_1-X_1 System

A study of the spectrum excited by the 514.5-nm Ar$^+$ line (Fig. 2) shows that the
laser simultaneously excited two transitions in the same system, leading to two
vibrational progressions of PQR triplets. As there were two anti-Stokes com-
ponents in one progression and one in the other, and most of the intensity resides
in the first anti-Stokes group, it was concluded that the laser excited the 0, 1
(P branch) and 1, 2 (R branch) bands. Photographic wavelength and frequency
measurements are listed in Table II. From the P, R separations, it was calculated
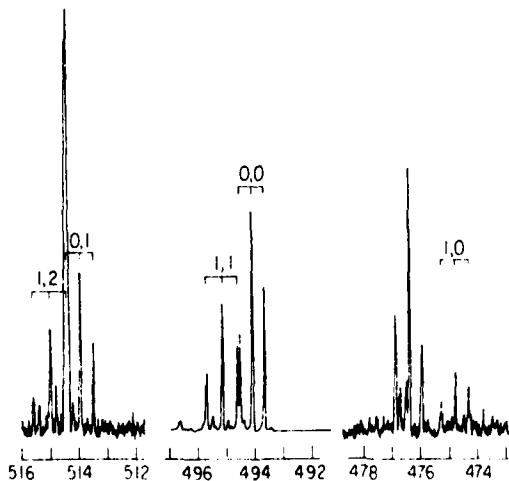
Fig. 2. Portions of the fluorescence spectrum of CeO excited by the Ar$^+$ 514.5-nm laser line at a
pressure of 1 Torr. Wavelengths are in nanometers and the labeled lines belong to the $C_1(1)-X_1(2)$
system. The detector sensitivity was decreased by a factor of 10 for the 492-496 nm region.

TABLE II

Photographic Measurements of $C_1(3)-X_1(2)$ Fluorescence Lines Excited by the Ar^+ 514.5-nm Line

Wavelength (nm)[*]	Wavenumber (cm^{-1}) Observed	Ref. 7	Assignment
474.412	21 072.8		R(29) 1,0
474.890	21 051.6		Q(30) 1,0
475.384	21 029.7		P(31) 1,0
492.768	20 287.9	20 288.0	R(23) 0,0
493.181	20 270.9	20 271.0	Q(24) 0,0
493.612	20 253.2	20 253.3	P(25) 0,0
493.702	20 249.5		R(29) 1,1
494.220	20 228.3		Q(30) 1,1
494.751	20 206.3		P(31) 1,1
513.59[+]	19 465.4[+]		R(23) 0,1
514.065	19 447.4		Q(24) 0,1
514.532	19 429.7		P(25) 0,1
514.532	19 429.7		R(29) 1,2
515.096	19 408.4		Q(30) 1,2
515.69[+]	19 386.1[+]		P(31) 1,2

[*]Relative accuracy 0.005 nm, 0.2 cm^{-1}.

[+]Photoelectric measurements not used in calculations, relative
accuracy 0.025 nm, 1.0 cm^{-1}.

that the laser excited $P(25)$ of the 0-1 band and $R(29)$ of the 1-2 band. The R lines were more intense than the P lines, suggesting that $\Delta\Omega = +1$. Comparison with high resolution data (7) showed that the 0-0 lines are in good agreement with the measured frequencies of the $R(23)$, $Q(24)$, and $P(25)$ lines of the 0-0 band of the $C_1(3)-X_1(2)$ transition.

For the X_1 state, Eq. (1) was used to calculate vibrational spacings. $\Delta G_{v+1,2}$, from which vibrational constants were derived in the usual way (10). As α_e was not determined for this state, a first approximation to the constants was obtained by ignoring α_e in Eq. (1). The Pekeris formula was used to estimate α_e (~0.0011 cm^{-1}) which was then used in Eq. (1) to improve the constants.

The vibrational spacing in the C_1 state was determined by making use of two pieces of experimental information.

(i) $P_{01}(25) = R_{12}(29)$ (coincident transitions at the laser wavelength).
(ii) $P_{00}(25) = R_{11}(29) + 3.7$ cm^{-1}.

Values of $\nu_{01} - \nu_{12}$ and $\nu_{00} - \nu_{11}$ were derived and used together with the X_1 state vibrational spacings, to calculate $\Delta G'_{1,2}$. The results are listed in Table IV. The values derived for $\nu_{00} - \nu_{11}$ and $\nu_{01} - \nu_{12}$ are slightly dependent on the value chosen for α_e, but it was found that varying α_e through its expected range from 0.001 to 0.002 cm^{-1} only made a difference of 1 cm^{-1} to the value of $\Delta G'_{1,2}$.
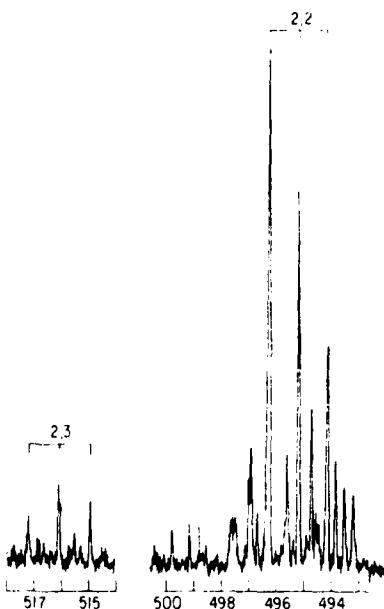
FIG. 3. Portions of the fluorescence spectrum of CeO excited by the Ar^+ 496.5-nm laser line at a pressure of 1 Torr. Wavelengths are in nanometers and the labeled lines belong to the $C_1(3)-X_1(2)$ system.

The three lines around 476.5 nm (Fig. 2) were shown, by tuning the etalon, to be excited simultaneously with $v = 1$ of the C_1 state and not with $v = 0$. As they do not fit into any progressions they probably involve a different low lying state.

Portions of the very complex spectrum excited by the 496.5-nm line are shown in Fig. 3. The two marked triplets appear to belong to a progression. Wavelengths and frequencies, which were measured from fast photoelectric scans and are thus only accurate to ± 3 cm^{-1}, are listed in Table III. The lines have been assigned to the 2-2 and 2-3 bands of the C_1-X_1 system with the laser exciting $P(61)$ of the

TABLE III

Photoelectric Measurements of $C_1(3)-X_1(2)$ Fluorescence Excited by the Ar^+ 496.5-nm Line

Wavelength (nm)*	Wavenumber (cm^{-1})	Assignment
494.41	20 220.5	R(59) 2,2
495.43	20 178.9	Q(60) 2,2
496.51	20 135.0	P(61) 2,2
515.02	19 411.3	R(59) 2,3
516.14	19 369.2	Q(60) 2,3
517.24	19 328.0	P(61) 2,3

*Relative accuracy 0.08 nm, 3.0 cm^{-1}

CeO FLUORESCENCE   435

2–2 band. To within measured accuracy, there is reasonable agreement between observed and calculated frequencies for these lines.

CONCLUSION

The work described above illustrates the power of the fluorescence technique in providing vibrational information on the CeO molecule, especially when used in conjunction with high resolution absorption measurements. Vibrational spacings in the X_1, X_3, C_1, and D_3 states obtained from frequency measurements differ from values calculated from the Kratzer relation by as much as 65 cm^{-1} (Table IV). The intensity distribution within the PQR groups confirmed that both C_1-X_1 and D_3-X_3 are $\Delta\Omega = +1$ transitions. The measured relative intensities were also found to be consistent with the Ω numbering of Barrow et al. (5).

Calculation of vibrational constants, as opposed to vibrational spacings, tends to be hampered by the fact that, in all our observed spectra, vibrational progressions are short, generally involving only $\Delta v = 0$, ± 1 sequences. This is because the potential curves lie almost directly above each other with the result that nearly all the intensity is concentrated in the $\Delta v = 0$ sequence. This also means that B values for all the states are similar, as shown by the fact that transitions to different electronic states have almost the same PQR separations.

Evidence for transitions to previously unobserved electronic states has been mentioned briefly in the previous section. The unassigned lines in Figs. 1 and 2 show the probable presence of states close to the X_3 and X_1 states. In addition, a group of lines around 764 nm was observed with 514.5-nm excitation, indicating that there is probably a state about 6350 cm^{-1} above the X_1 state. While these states have not yet been assigned to known states, the presence of several new electronic transitions in nearly all observed fluorescence spectra suggest that important electronic as well as vibrational information will be obtained from our spectra.

The results presented here represent a small fraction of the data that we have accumulated. Fluorescence spectra have been excited at several wavelengths,

TABLE IV

Constants Obtained for the $X_1(2)$, $X_3(4)$, $C_1(3)$, and $D_3(5)$ States of CeO

Constant (cm^{-1})	X_1	X_3	C_1	D_3
$\Delta G_{1/2}$	824.3 (1)	822.1 (3)	783.6 (3)	785.7 (5)
$\Delta G_{3/2}$	820.9 (')			
ω_e	827.7 (2)			
ω_e (ref. 5)*	851	887	757	813
$\omega_e x_e$	1.7 (1)			
ω_e (Peker's)	0.0011			

*Calculated from Kratzer relation, $\omega^2 = 4B^3/D$

Numbers in parentheses represent the standard deviation in the last digit.

436   LINTON, DULICK, AND FIELD

excitation spectra have been obtained using a dye laser in the Rhodamine 6G
region, and double resonance excitation spectra have been obtained using Ar⁺
and dye lasers simultaneously. Analysis is continuing with a view to linking more
fluorescence transitions to known states and fitting all observed spectra into
a comprehensive energy level diagram.

ACKNOWLEDGMENTS

RECEIVED: January 17, 1979

REFERENCES

1. S. WYCKOFF AND P. A. WEHINGER, *Astrophys. J.* **212**, L139 (1977).
2. S. WYCKOFF AND R. E. S. CLEGG, *Mon. Not. Roy. Astronom. Soc.* **184**, 127–143 (1978).
3. R. E. S. CLEGG AND D. L. LAMBERT, *Astrophys. J.* **226**, 931–936 (1978).
4. A. GATTERER, J. JUNKES, E. W. SALPETER, AND B. ROSEN, "Molecular Spectra of Metallic
   Oxides," Specola Vaticana, Vatican City.
5. R. F. BARROW, R. M. CLEMENTS, S. M. HARRIS, AND P. P. JENSON, *Astrophys. J.* **229**,
   439–447 (1979).
6. L. L. AMES AND R. F. BARROW, *Proc. Phys. Soc.* **90**, 869–870 (1967).
7. R. M. CLEMENTS, D. PHIL. Thesis, Oxford University, 1969.
8. R. L. DEKOCK AND W. WELTNER, JR., *J. Phys. Chem.* **75**, 514–525 (1971).
9. J. B. WEST, R. S. BRADFORD, JR., J. D. EVERSOLE, AND C. R. JONES, *Rev. Sci. Instrum.* **46**,
   165–168 (1975).
10. G. HERZBERG, "Spectra of Diatomic Molecules," Von Nostrand, New York, 1950.

NOTES

On the Hyperfine Structure of the 0–0 Band in the PrO XVII System[1]

Beaufils *et al.* (*1*) observe (at resolution no better than 0.07 cm^{-1}) hyperfine splittings at low J values in the 0–0 band of the XVII system of PrO (*2*). They conclude that the dominant hyperfine splitting originates in the lower electronic state of the XVII system. We have examined this system at considerably higher, Doppler-limited, resolution (0.002 cm^{-1}) by recording excitation spectra with a 1-MHz-bandwidth cw dye laser capable of continuous 30-GHz scans. We conclude, from measurements of low-J lines in both R and P branches, that the dominant hyperfine splitting is in the upper state.

PrO is produced by heating Pr_6O_{11} with a trace of Pr metal to 1300–1400°C in a graphite crucible. The vaporized PrO is entrained in flowing Ar at 1–3 Torr. Fluorescence is excited with a Coherent Radiation Model 599-21 (Rhodamine 6G) dye laser, dispersed through a 1-m Spex Model 1802 monochromator at a spectral bandwidth of approximately 0.1 nm, and detected by a dry-ice-cooled Hamamatsu Model R818 photomultiplier. The monochromator wavelength setting is adjusted to selectively detect Q-branch fluorescence resulting from R- or P-branch excitation, thereby eliminating scattered laser light and extraneous excitation lines belonging to other band systems. The resultant

TABLE I

Frequencies of Completely Resolved Hyperfine Components of $R(4.5)$, $P(6.5)$, and $R(6.5)$ Lines of XVII 0–0 Band

R(4.5)			P(6.5)				R(6.5)		
F'	ν(F',J'=5.5)	$\Delta\nu$	F'	ν(F',J'=5.5)	$\Delta\nu$	F"	F"	ν(F",J"=6.5)	$\Delta\nu$
3	16 594.769		3	16 586.109		4	4	16 596.075	
		0.066			0.068				0.054
4	16 594.835		4	16 586.177		5	5	16 596.129	
		0.083			0.084				0.063
5	16 594.918		5	16 586.261		6	6	16 596.192	
		0.100			0.096				0.075
6	16 595.018		6	16 586.357		7	7	16 596.265	
		0.116			0.116				0.080
7	16 595.134		7	16 586.473		8	8	16 596.345	
		0.132			0.130				0.090
8	16 595.266		8	16 586.603		9	9	16 596.435	

334   NOTES
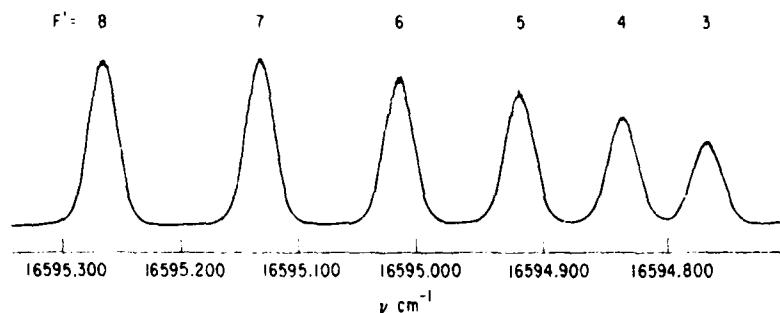

FIG. 1. A segment of the PrO XVII 0–0 excitation spectrum showing the R(4.5) line.

fluorescence excitation spectrum is calibrated with respect to I_2 $B0^+_u-X\Sigma^+_g$ lines (3) by simultaneously recording I_2 and PrO excitation spectra. PrO hyperfine lines are recorded at ±0.003-cm^{-1} accuracy.

Frequencies of completely resolved hyperfine components of the R(4.5), P(6.5), and R(6.5) lines of the XVII 0–0 band are listed in Table 1. Since the R(4.5) and P(6.5) lines have a common upper rotational level, agreement of hyperfine splittings within these two lines to within the ±0.003-cm^{-1} measurement uncertainty demonstrates that the dominant splitting occurs in the upper electronic state. This is confirmed by the completely different splittings found for the P(6.5) and R(6.5) lines which have a lower rotational level in common. Similar agreement between hyperfine splittings is found for all pairs of $P(J''-1)$ and $R(J''+1)$ lines for which hyperfine components are clearly resolved. The structure of the R(4.5) line is illustrated in Fig. 1.

The fact that the hyperfine splitting of the lower electronic state is much smaller than that of the upper state implies that the lower-state configurational assignment of Beaufils et al. (1), $^2\Gamma$ Pr$^+$O$^-(\phi4f)^3(\sigma6s)(\pi2p)^3$, is incorrect. The half-filled σ orbital, located predominantly on the Pr nucleus, should result in a large hyperfine splitting.

A complete rotation and hyperfine analysis of the PrO XVII system will be reported subsequently.

REFERENCES

1. J. Cl. BEAUFILS, P. CARETTE, AND J. M. BLONDEAU, J. Mol. Spectrosc. 77, 1–10 (1979).
2. E. A. SHENYAVSKAYA, I. V. EGOROVA, AND V. N. LUPANOV, J. Mol. Spectrosc. 47, 355–362 (1973).
3. S. GERSTENKORN AND P. LUC, "Atlas du Spectre d'Absorption de la Molécule d'Iode," CNRS, Paris, 1978.

MICHAEL DULICK, ROBERT W. FIELD, AND J. CL. BEAUFILS[2]

Department of Chemistry and Spectroscopy
  Laboratory
Massachusetts Institute of Technology
Cambridge, Massachusetts 02139

[2] Visiting Scientist, U.E.R. de Physique Fondamentale, Université de Lille(I), B.P. 36, 59650 Villeneuve d'Ascq, France.

Low lying electronic states of CeO

C. Linton

Physics Department, University of New Brunswick. Fredericton. New Brunswick, Canada E3B 5A3

M. Dulick and R. W. Field

Department of Chemistry and Spectroscopy Laboratory, Massachusetts Institute of Technology, Cambridge, Massachusetts 02139

P. Carette

U.E.R. de Physique Fondamentale, Universite de Lille I, 59655 Villeneuve D'Ascq., France

R. F. Barrow

Physical Chemistry Laboratory. Oxford University. South Parks Road, Oxford, OX1 3QZ, England
(Received 28 July 1980; accepted 28 August 1980)

A summary is given of the results of laser induced fluorescence experiments on the CeO molecule, which result in the determination of the relative energies of seven low lying electronic states. Both argon ion and cw dye lasers were used to excite several transitions from the $X_1(\Omega = 2)$, $X_2(\Omega = 3)$, and $X_3(\Omega = 4)$ states and the resulting fluorescence spectra showed that (i) the $X_2(3)$ state is 80.4 ± 0.7 cm^{-1} above $X_1(2)$, (ii) $X_4(3)$ is 100.6 ± 1.5 cm^{-1} above $X_3(4)$, and (iii) there are three states labeled $u(2), w(3), v(2)$, which are 834, 2537, and 2688 (± 3) cm^{-1} respectively above $X_2(3)$. It was also shown that the vibrational frequencies $\Delta G_{1,2}$, of the seven low lying states are all between 820 and 825 cm^{-1}.

INTRODUCTION

The electronic structures of diatomic molecules with partially filled d and f orbitals are only fragmentarily known. The reason for this is the huge number of low-lying molecular states with nearly identical rotational and vibrational constants which arise from numerous, nearly isoenergetic, nonbonding orbitals. Either by accident or selection rule, many low-lying states remain undiscovered and the relative energies of known states remain undetermined. The CeO molecule belongs in this category and there has been increasing interest in its spectrum following the discovery of CeO bands in absorption spectra of S-type stars.[1-3]

The ground state of LaO is known to be $(\ldots\ldots\sigma)$, $^2\Sigma^+$ while that of CeO has not yet been established. However, with one electron more than LaO, CeO could have as many as sixteen low-lying states, $\Omega = 0^+$ (two), 0^- (two), 1 (three), 2 (four), 3 (four), and 4 (one), all components of the configuration $(\ldots\ldots\sigma)$ $(4f\ldots)$. Other possible configurations would give even more states. For this kind of molecule, the methods of classical spectroscopy, in which gas phase absorption and emission spectra are recorded at Doppler limited resolution, may be tedious and even ineffectual.

Of some forty bands of CeO which have been analyzed rotationally,[4,5] many involve transitions to one of four low-lying electronic states, $X_1(\Omega = 2)$, $X_2(3)$, $X_3(4)$, and $X_4(3)$. At least four other low lying states have also been observed. However, because of the lack of observed transitions from common upper states, the only information so far established about relative energies of these states is that the $X_4(3)$ state is 2060 cm^{-1} above $X_2(3)$. Information on vibrational frequencies is also scarce, only that of the $X_2(3)$ state having been determined from rotational analysis.

It is becoming clear that major progress in unravelling the interrelations of low lying states in manifolds of this kind can result from studies of laser induced fluorescence. The high degree of specificity of the excitation process combined with the excellent signal/noise ratio in the detection of fluorescence leads to the possibility of recognizing weak more or less forbidden transitions in the presence of much stronger allowed systems. This leads to the expectation that complete level diagrams for the lowest states of d and f electron molecules may be constructed. Recent laser fluorescence experiments[6] have led to determination of vibrational frequencies for the $X_1(2)$ and $X_3(4)$ states, and illustrate the value of the technique. We now report the electronic energy level scheme linking seven low lying states of CeO, and vibrational frequencies of these states, all of which have been derived from the results of an extensive series of laser experiments.

EXPERIMENTS

The results reported here are based mainly on a series of laser-induced fluorescence experiments. These were backed up by further experiments involving rotational analysis of high resolution emission and absorption spectra.

The source used in all the laser experiments was a Broida oven[6,7] in which either a heated mixture of Ce and CeO$_2$ or the reaction of Ce vapor with O$_2$ was used to make CeO. Fluorescence was excited using an argon ion laser and a dye laser with dyes covering the 460-480 and 580-615 nm regions. Low to medium resolution (≥ 0.025 nm) spectra were recorded on 0.5 and 1 m monochromators.

Fluorescence was excited in transitions which have previously been rotationally analyzed and for which, in

TABLE I. Electronic transitions of CeO excited in laser fluorescence experiments.

Excited transition	Band head wavelength (nm)	Observed fluorescence transitions
$h_2(3)-u(2)$ 0,0	463.13	$h_2(3)-X_2(3)$, $u(2)$, $X_4(3)$, $v(2)$
$g_2(2)-X_2(3)$ 0,0	476.48	$g_2(2)-X_2(3)$, $u(2)$, $X_4(3)$, $v(2)$
$e_2(3)-X_2(3)$ 0,0	584.37	$e_2(3)-X_1(2)$, $X_2(3)$, $u(2)$, $X_3(4)$, $X_4(3)$, $v(2)$
$B_1(2)-X_1(2)$ 0,0	604.58	$B_1(2)-X_1(2)$, $X_2(3)$, $u(2)$, $X_4(3)$, $w(3)$, $v(2)$
$E_2(4)-X_2(3)$ 0,0	608.03	$E_2(4)-X_2(3)$, $u(2)$, $X_3(4)$, $X_4(3)$, $w(3)$
$E_2(4)-X_2(3)$ 1,1	611.59	
$C_3(4)-X_3(4)$ 0,0	611.19	$C_3(4)-X_2(3)$, $X_3(4)$, $X_4(3)$, $w(3)$

most cases, the lower state was known. Detailed line lists[8] were then used to check the assignment of the laser transition. Two bands, with heads at 476.48 and 584.37 nm, and which had not previously been analyzed, were photographed at high resolution and analyzed. Both emission (hollow cathode) and absorption (King furnace) sources were used.

RESULTS

Transitions excited in the laser fluorescence experiments are listed in Table I. The 476.48 nm band was excited by the argon laser line at 476.49 nm. In the other bands, which were excited by the dye laser, several different rotational transitions were examined. The $F_2(4)-X_2(3)$ 1–1 band has not been rotationally analyzed and its assignment was based on the fluorescence spectra.

The spectra typically consisted of doublets (RP) or triplets (RQP), sometimes forming vibrational progressions and sometimes distributed randomly throughout the spectrum indicating transitions to different low-lying electronic states. The J value of the upper state was determined in the usual manner from measured separations of the P and R lines in a doublet or triplet. Doublets or triplets with the same RP separation and separated by ~820 cm^{-1}, which is typical of vibrational frequencies of low-lying CeO states[4,6] were assigned to vibrational progressions. Relative intensities of R, Q, and P lines were used to determine whether $\Delta\Omega(=\Omega'-\Omega'')$ were +1, 0, or −1 for each observed transition. As Ω' and Ω'' were usually known for the transition excited by the laser, the Ω values of the other low lying states in the fluorescence spectrum could be determined. Care had to be taken as perturbations caused many anomalies which affect the relative intensities of R and P lines, but these disappeared at low J (as required by the heterogeneous perturbation mechanism) enabling us to assign $\Delta\Omega$ correctly.

For each transition excited, the separations of the various RP and RQP groups in the fluorescence spectrum led to the construction of an energy level diagram consisting of one known electronic state and several other states whose Ω values had been established as above. All the individual energy diagrams were then examined for recurrence of states with a common separation and matching Ω values. For example, $B_1(2)$, pumped by a transition in $B_1(2)-X_1(2)$, fluoresces to a state $\Omega=3$ at

80 cm^{-1} above $X_1(2)$, and $e_2(3)$, pumped in $e_2(3)-X_2(3)$, fluoresces to a state $\Omega=2$ at 80 cm^{-1} below $X_2(3)$, thus linking the $X_1(2)$ and $X_2(3)$ states. Similar coincidences were found to link the $X_3(4)$ and $X_4(3)$ states. In each case, the characteristic 2060 cm^{-1} separation was used to check for the presence of the $X_2(3)$ and $X_4(3)$ states. The energy spacing between each state and either the $X_2(3)$ or $X_4(3)$ state was measured and these are listed as characteristic separations in Table II. All states were then placed on the same energy scale.

The resulting energy level diagram, shown in Fig. 1, contains 7 states whose energies relative to $X_1(2)$, are listed in Table II. All the listed states were established from at least two independent laser-induced transitions, and all the measurements were used in calculating the energies. Because of the scatter in the low resolution data, and the very small variation of electronic state separation as a function of J (due to the near equality of the rotational constants), some energy separations are averaged values and not extrapolated to $J=0$. For three pairs of states, $X_1(2)$ and $X_2(3)$, $X_3(4)$ and $X_4(3)$, $X_4(3)$

TABLE II. Energies and vibrational frequencies of low-lying CeO states.

State	Characteristic separation (cm^{-1})	Energy (cm^{-1})	$\Delta G_{1/2}$ (cm^{-1})	Note
$v(2)$	$v-X_4=628.1$ (15)	2768.7 (21)	823.4 (19)	1, 2
$w(3)$	$w-X_4=476.7$ (11)	2617.3 (19)	825.0 (03)	3
$X_4(3)$	$X_4-X_2=2060.3$	2140.6 (15)	823.1 (07)	4, 5
$X_3(4)$	$X_4-X_3=190.5$ (15)	2040.1 (21)	822.1 (03)	2, 6
$u(2)$	$u-X_2=833.9$ (28)	914.2 (32)	823.0 (04)	7
$X_2(3)$	$X_2-X_1=80.3$ (15)	80.3 (15)	822.8	2, 3, 8
$X_1(2)$		0	824.3 (01)	6

Notes: (1) Numbers in parentheses represent the standard deviation in the last two digits.

(2) Characteristic separation has been extrapolated to $J=0$

(3) $\omega_e x_e = 2.2+0.9$ cm^{-1}.

(4) Characteristic separation is from Barrow et al.[4]

(5) $\omega_e x_e = 2.4+1.1$ cm^{-1}.

(6) $\Delta G_{1/2}$ is from Linton et al.[6]

(7) $\omega_e x_e = 1.6+0.7$ cm^{-1}.

(8) $\Delta G_{1/2}$ is from Barrow et al.[6]
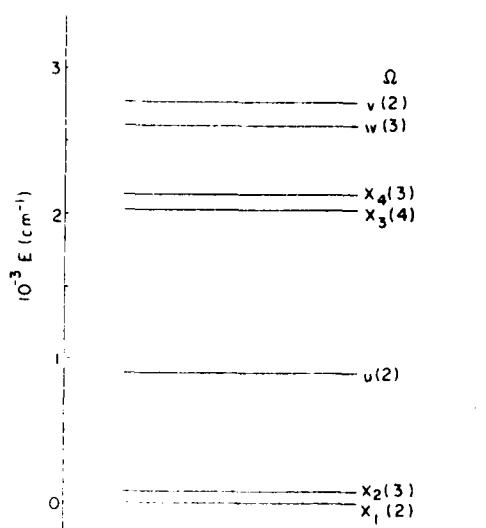
FIG. 1. Low-lying energy states of CeO.

lying states, $u(2)$, $v(2)$, and $w(3)$, have been observed and their energies determined. These have not yet been identified with any of the states listed by Barrow *et al.*[4] and none of the lower states of the absorption transitions, l, m, n, and o have been identified in fluorescence spectra. Further work, either in the study of fluorescence from the upper states of systems, l, m, n, and o, or by rotational analysis of bands involving states u, v, and w will be required to elucidate the relations between these states.

We have reported here an outline of our experiments and the final conclusions. A great deal of information has been obtained from these experiments and details of the experiments, results and analysis will be presented in a future publication.

ACKNOWLEDGMENTS

and $v(2)$, the separations showed definite J dependence and were extrapolated to $J = 0$.

Vibrational frequencies are also listed in Table II. Those of the $X_1(2)$, $X_2(3)$, and $X_3(4)$ states are from previous experiments.[4,6] Because of the scatter in the data, it was not possible to derive accurate vibrational constants and only $\Delta G_{1/2}$ is listed in the table. The states for which more than two vibrational levels were observed are noted together with approximate values of $\omega_e x_e$. It is clear from the results that the vibrational frequencies of all the low-lying states are very similar.

CONCLUSIONS

The most important result of this work has been the establishment of the relative energies of the $X_1(2)$, $X_2(3)$, $X_3(4)$, and $X_4(3)$ states. In addition, three other low-

[1]S. Wyckoff and P. A. Wehinger, Astrophys. J. Lett. **212**, 139 (1977).

[2]S. Wyckoff and R. E. S. Clegg, Mon. Not. R. Astron. Soc. **184**, 127 (1978).

[3]R. E. S. Clegg and D. L. Lambert, Astrophys. J. **226**, 931 (1978).

[4]R. F. Barrow, R. M. Clements, S. M. Harris, and P. P. Jenson, Astrophys. J. **229**, 439 (1979).

[5]P. Carette (unpublished work).

[6]C. Linton, M. Dulick, and R. W. Field, J. Mol. Spectrosc. **78**, 428 (1979).

[7]J. B. West, R. S. Bradford, Jr., J. D. Eversole, and C. R. Jones, Rev. Sci. Instrum. **46**, 165 (1975).

[8]R. M. Clements, Thesis, Oxford, 1969.

The Spectrum of CuO: Low Lying Electronic States Observed by Laser Induced Fluorescence

O. Appelblad, A. Lagerqvist and I. Renhorn*

Institute of Physics, University of Stockholm, Vanadisvägen 9, S-113 46 Stockholm, Sweden

R. W. Field

Department of Chemistry and Spectroscopy Laboratory, Massachusetts Institute of Technology, Cambridge, Massachusetts 02139, U.S.A.

Abstract

The spectrum of gas phase CuO in the red and near infra-red wavelength region is studied by the laser induced fluorescence technique. Three new low lying electronic states, $\alpha\Sigma$, $\gamma^2\Pi_i$ and $\delta^2\Sigma$, with the approximate T_0 values

$\alpha\Sigma$	$15\,424\ \text{cm}^{-1}$
$\gamma^2\Pi_{1,2}$	$15\,470\ \text{cm}^{-1}$
$\gamma^2\Pi_{3/2}$	$15\,166\ \text{cm}^{-1}$
$\delta^2\Sigma$	$12\,986\ \text{cm}^{-1}$

are reported. The multiplicity of the $\alpha\Sigma$ is uncertain. It is tentatively considered to be a quartet. The vibrational constants of the $\delta^2\Sigma$ state are

$$\omega_e \sim 661\ \text{cm}^{-1} \quad \text{and} \quad \omega_e x_e \sim 5.7\ \text{cm}^{-1}.$$

Earlier results on the spectrum of CuO are reviewed. Intensity anomalies, originating from interference between groups of states, are discussed.

1. Introduction

The emission spectrum of gaseous copper oxide, CuO, possesses many electronic transitions in the wavelength region between 4000 Å and 6500 Å. In the last few years most of these systems have been rotationally analyzed. The most characteristic band system for the molecule is the one located by itself in the orange-red region. In the region from 4200 Å to 4800 Å the large number of bands gives the spectrum a very complicated appearance.

As early as 1912 Hertenstein [1] reported measurements of band heads which he believed belong to CuO. Attempts to perform vibrational analyses have been made by a number of authors [2–5]; but all of them are incorrect. In 1968 Antić-Jovanović et al. [6] performed a vibrational analysis of the orange-red system from a study of the isotopic molecules Cu ^{16}O and Cu ^{18}O. In some important points it was, however, erroneous [7]. Antić-Jovanović and Pešić [8] later performed a rotational analysis of this system. Their analysis is also incorrect.

The first correct analysis of a CuO system was made in 1967 by Lagerqvist and Uhler [9] who treated a single band at 4182 Å. The band had the appearance of a $^2\Pi_{3/2}-^2\Pi_{3/2}$ transition. Later this band was ascribed as belonging to a system labelled $M\,^2\Pi_{3/2}-X\,^2\Pi_{3/2}$. In a recent paper [10] a more detailed treatment is given of this band. A rotational analysis of the $F^2\Pi_i-X^2\Pi_i$ system at 4711 Å and 4770 Å was performed in 1973 by Appelblad and Lagerqvist [11]. A more detailed analysis of this system and also an analysis of the orange-red

system at 6045 Å and 6147 Å, $A\,^2\Sigma-X\,^2\Pi_i$, were given in 1974 by the same authors [7]. In 1975 a study of the $G\,^2\Pi_i-X\,^2\Pi_i$ transition at 4629 Å and 4687 Å was reported [12]. In 1976 [13], four new band systems, $E^2\Delta-X^2\Pi_i$ at 4737 Å, $H\,^2\Pi$ $X^2\Pi_i$ at 4606 Å, $I^2\Pi-X^2\Pi_i$ at 4452 Å and $P^2\Pi-X^2\Pi_i$ at 4286 Å, were presented. Further a survey of all electronic states analyzed at that time was given. The $C^2\Pi_i-X^2\Pi_i$ system at 5312 Å and 5345 Å, earlier studied by Lefebvre et al. [14], was also included in this survey. The analysis of the 5345 Å band in [14] was however not correct. A re-analysis of the $C^2\Pi_i-X^2\Pi_i$ system and an analysis of the $D^2\Delta_i$ $X^2\Pi_i$ system at 5326 Å and 5274 Å were published in 1978 by Appelblad et al. [15]. Recently two new band systems, $A'^2\Sigma$ $X^2\Pi_i$ at 6430 Å, Lefebvre et al. [16], and a $^2\Delta_i-X^2\Pi_i$ system at 6522 Å and 6493 Å, Pinchemel et al. [17], have been reported.

One quartet–doublet transition has been found, namely a band system at 4432 Å, which has been interpreted as a $^4\Sigma_{1/2}-X^2\Pi_{1/2}$ transition [18].

The molecular constants of the ground state are, in cm^{-1}, $\omega_e \sim 640$ ($^2\Pi_{3/2}$), $\omega_e \sim 636$ ($^2\Pi_{1/2}$), $B_e \sim 0.444$ and $A \sim -277$. The constants ω_e and B_e are smaller for all other systems with the following exceptions: $A\,^2\Sigma$, $\omega_e \sim 643$; $C^2\Pi_{3/2}$, $\omega_e \sim 658$; $E^2\Delta_{5/2}$, $\omega_e \sim 734$ and $B_e \sim 0.445$.

The purpose of the present investigation was to search for new low lying electronic states in CuO. In this paper we report on three new low lying states. All three systems involve the $X^2\Pi_i$ state. From band profiles and intensity considerations we believe that the electronic symmetry of the states are Σ (multiplicity uncertain), $^2\Pi_i$, and $^2\Sigma$ respectively. We here lable them $\alpha\Sigma$, $\gamma^2\Pi_i$, and $\delta^2\Sigma$. Approximate vibrational constants have been determined for the $\delta^2\Sigma$ state. They are: $\omega_e \sim 661\ \text{cm}^{-1}$ and $\omega_e x_e \sim 5.7\ \text{cm}^{-1}$. Thus, below the $A'^2\Sigma$ state, four states are known, namely the $\beta^2\Delta_i$ state [17] and the three new states $\alpha\Sigma$, $\gamma^2\Pi_i$, and $\delta^2\Sigma$ reported here. The T_0 values estimated from band heads are, in cm^{-1}

α	Σ	15 424
$\beta^2\Delta_{5/2}$		15 317
$\beta^2\Delta_{3/2}$		15 665
$\gamma^2\Pi_{3/2}$		15 166
$\gamma^2\Pi_{1/2}$		15 470
$\delta^2\Sigma$		12 986.

The T_0 value of the $\beta^2\Delta_{5/2}$ state is obtained from rotational analysis [17].

2 Experimental

The copper oxide molecule was formed in a Broida type high temperature flow system [19]. Copper was melted in a resistively heated aluminum oxide crucible. By insulating the crucible with zirconia cloth, hot spots were avoided and a temperature around 1600° C could be conveniently used. The copper vapour was carried into the reaction chamber by an Ar gas stream. The Ar pressure was varied from 1–10 torr.

In the reaction chamber N_2O was injected and a weak reddish flame was observed. The oven assembly used in this experiment has been described in several papers [19–22]. Radiation from a dye laser, pumped by an Ar^+ laser, was directed vertically into the reaction chamber. Three different dyes were used in the experiment. The $A'-X$ system around 6500 Å was excited by rhodamine B, the $A-X$ system around 6100 Å by rhodamine 6G, and the $C-X$ and $D-X$ systems around 5300 Å by rhodamine 110. The dye laser was tuned by a three stage birefringent filter giving a bandwidth of approximately 1 cm^{-1}. The laser induced fluorescence was spectrally resolved by a SPEX 1802 1-meter monochromator fitted with a 1200 grooves/mm grating blazed at 1.2 μm, a Hamamatsu R 818 red sensitive photomultiplier, and a picoammeter-recorder system. Excitation spectra were also observed by detecting the laser induced fluorescence through a spatial filter while the laser was tuned over the wavelength region of interest. In this mode of operation, very weak transitions were observed free of interference from laser scatter and chemiluminescence. The emission spectrum was recorded between 4000 and 9000 Å and lines from mercury and neon pen lamps were used for calibration.

Supplementary studies of the low lying states have been made using a composite wall hollow cathode discharge [10] and a scanning monochromator (Jobin Yvon HR 1500). At these studies a Hamamatsu R 955 photomultiplier and a photon counting recorder system were used.

3. The excitation spectrum

Several band systems are, as described in Section 2, within the tuning range of Ar$^+$-pumped cw dye laser. Laser excitation spectroscopy can be used in order to estimate the molecular population of various vibronic states [23]. A strong absorption of the laser light may indicate that the lower level is the ground state, although it might also be a metastable state populated in a chemical reaction. All the known electronic transitions from $X^2\Pi$ which fall within the tuning range of the laser, 5300–6600 Å, have been observed by laser excitation spectroscopy. No laser excitation transitions were found in this region which did not involve the $X^2\Pi$ state. The absence of transitions out of other low-lying states for a molecule with such a high density of electronic states is a strong argument that the CuO $X^2\Pi_i$ state is the electronic ground state.

Laser induced fluorescence has been recorded in different ways. The excitation spectrum of the $A^2\Sigma-X^2\Pi_i$ system, shown in Fig. 1, was recorded by detecting undispersed laser induced fluorescence through a spatial baffle system, which was found to be very effective in reducing chemiluminescence and scattered laser light.

The spectrum shown in Fig. 2 was obtained by laser exciting the $A^2\Sigma$ state, from which population was collisionally transferred into somewhat lower energy electronic states. The pumping laser was kept at a fixed frequency and the monochromator scanned over the region shown. Since the $A-X$

Fig. 1. Laser excitation spectrum of the $A^2\Sigma-X^2\Pi_i$ band system (uncorrected for laser intensity or detector response). Laser induced fluorescence was detected through a spatial baffle system while the laser was scanned. Since laser intensity was not constant over the tuning range, the $A^2\Sigma-X^2\Pi_{1/2}$ system misleadingly appears to be weaker than the $A^2\Sigma-X^2\Pi_{3/2}$ system.

transition moment is quite large and the collisional relaxation very rapid, this excitation scheme was more efficient for obtaining emission spectra from the A', α, β, γ, and δ states than a direct excitation of these lower electronic states. The $A^2\Sigma-X^2\Pi_{1,2}$ $(\Delta v = -1)$, $A'^2\Sigma-X^2\Pi_i$ $(\Delta v = 0)$, $\beta^2\Delta_{3,2}-X^2\Pi_{1,2}$ $(\Delta v = 0)$ and $\beta^2\Delta_{5,2}-X^2\Pi_{3,2}$ $(\Delta v = 0)$ sequences are all present. The $A'-X$ and $\beta-X$ transitions are rather weak, but recently they have been partially rotationally analyzed [16, 17]. The $\beta^2\Delta_{3,2}-X^2\Pi_{1,2}$ sub-band is not yet analyzed. The intercombination band $\beta^2\Delta_{3,2}-X^2\Pi_{3,2}$ at 6379 Å can also be seen in Fig. 2. The large spin-rotation constant, γ, of the $A'^2\Sigma$ state and the presence of the 6379 Å sub-band both separately indicate the existence of at least one $^2\Pi$ state which lies close to $A'^2\Sigma$. A new band, without any obvious Q branch, (as expected for a $\Delta\Lambda = \Delta\Omega = 0$ transition) is located at 6575.8 Å. In addition, a very weak band is found at 6458 Å. The frequency difference between these two bands, 277 cm^{-1}, corresponds to the multiplet splitting of the ground state. It seems most likely that the band at 6575.8 Å is this predicted close lying $^2\Pi_{1,2}-X^2\Pi_{1,2}$ band. It is here called $\gamma^2\Pi_{1,2}-X^2\Pi_{1,2}$. The band at 6458 Å may then be interpreted as the intercombination band, $\gamma^2\Pi_{1,2}-X^2\Pi_{3,2}$. The oscillator strength of this sub-band evidently originates from an interaction with the $A'^2\Sigma$ state. This $A'\sim\gamma$ interaction probably also accounts for the large γ value of $A'^2\Sigma$. Since the $\gamma^2\Pi_{1,2}$ state is only about 50 cm^{-1} below the $A'^2\Sigma$ state, a rather small spin–orbit interaction $A'\sim\gamma$ can account for these effects. A sub-band at 6478.8 Å is tentatively interpreted as an $\alpha^4\Sigma-X^2\Pi_{3,2}$ transition. In Fig. 2 the positions of the band heads are marked.

The excitation spectrum shown in Fig. 3 was obtained by monitoring collisional relaxation into the $A'^2\Sigma$ state while scanning the laser. The monochromator was held fixed at the wavelength 6429.7 Å, the wavelength of the Q_1 head of the $A'^2\Sigma-X^2\Pi_{3,2}$ sub-band. In this spectrum, both sub-bands of the $\gamma^2\Pi_i-X^2\Pi_i$ transition can be observed as well as the $\alpha\Sigma-X^2\Pi_{1,2}$ transition. The wavelengths of the band heads are given in the figure.

Figure 4 shows the spectrum of the 7673 Å band obtained in the same way as the spectrum shown in Fig. 2. A sequence of band heads can be seen on the short wavelength side of the 7673 Å band. A weak band head is situated at 7840 Å. The frequency distance between the two bands again corresponds to the multiplet splitting of the ground state, $X^2\Pi$. The first impression of the bands is that they form a $^2\Sigma-X^2\Pi_i$ system where, in contrast to the usual situation of comparable sub-band intensities, the $^2\Sigma-X^2\Pi_{3/2}$ transition is much stronger
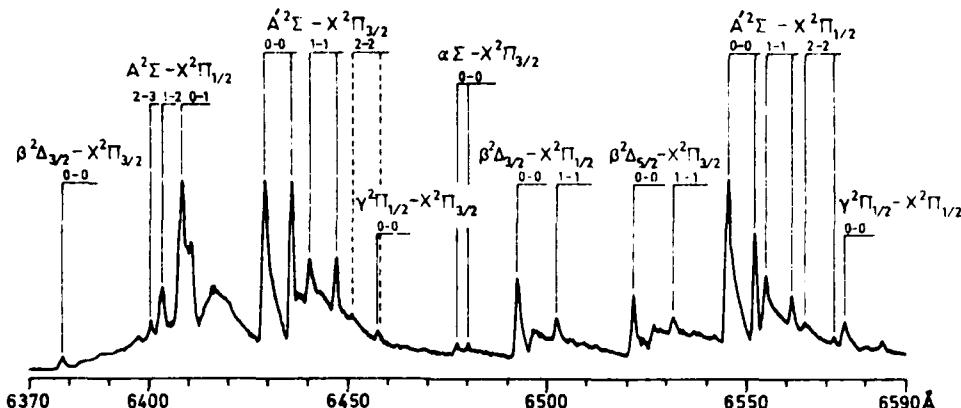
Fig. 2. Wavelength resolved laser induced fluorescence (uncorrected for spectrometer response). The observed electronic states are populated by relaxation from the $A\,^2\Sigma$ state. Transitions from five upper electronic states are recognized. The observed band systems are $A\,^2\Sigma-X\,^2\Pi_{1/2}$, $\Delta v = -1$ sequence, the $A'\,^2\Sigma-X\,^2\Pi_i$, $\alpha\Sigma-X\,^2\Pi_{3/2}$, $\beta\,^2\Delta_i-X\,^2\Pi_i$ and $\gamma\,^2\Pi_{1/2}-X\,^2\Pi_i$, $\Delta v = 0$ sequences.

than the $^2\Sigma-X\,^2\Pi_{1/2}$ transition. The Q head of the 7840 Å band should be the peak at 7866 Å, marked by $Q_{1/2}$ in the figure, and the Q heads of the 7673 Å bands should be the peaks at about 7695 Å, marked by $Q_{3/2}$. This intensity anomaly can most simply be explained as an interference effect arising from interaction between one $^2\Sigma^+$ state and one $^2\Sigma^-$ state, see Section 5. From the observed sequence of band heads at 7673 Å and with the knowledge of the vibrational spacing of the $X\,^2\Pi_{3/2}$ state, the $\Delta v = 1$ sequence can be predicted. The prediction is in agreement with the observed bands at 7309 Å. We tentatively name the system as $\delta\,^2\Sigma-X\,^2\Pi_i$.

4. Results

There has been some discussion concerning whether or not the $X\,^2\Pi_i$ state is the ground state of CuO. The results from the

matrix experiments by Shirk and Bass [24] cannot be easily interpreted in terms of known electronic states of gas phase CuO. On the other hand, if the known band systems of CuO, which all involve the $X\,^2\Pi_i$ state, could be obtained in an absorption experiment at relatively low temperature, then it would be reasonable to believe that the $X\,^2\Pi_i$ state is the ground state. In our study, excitation spectra of CuO are reported. This type of experiment is closely related to conventional absorption experiments. The vibrational temperature was about 400° C in the flame. The intensity of the observed excitation spectra and the fact that all bands observed involve the $X\,^2\Pi_i$ state indicate that $X\,^2\Pi_i$ is the ground state.

The most significant result of the laser induced fluorescence experiment is the observation of three new low lying electronic states. In Table I, the observed band heads of the $\alpha\Sigma-X\,^2\Pi_i$, $\gamma\,^2\Pi_i-X\,^2\Pi_i$ and $\delta\,^2\Sigma-X\,^2\Pi_i$ systems are listed as well as band heads from the $A\,^2\Sigma-X\,^2\Pi_i$, $\Delta v = -1$, $A'\,^2\Sigma-X\,^2\Pi_i$ and $\beta\,^2\Delta_i-X\,^2\Pi_i$, $\Delta v = 0$ sequences.
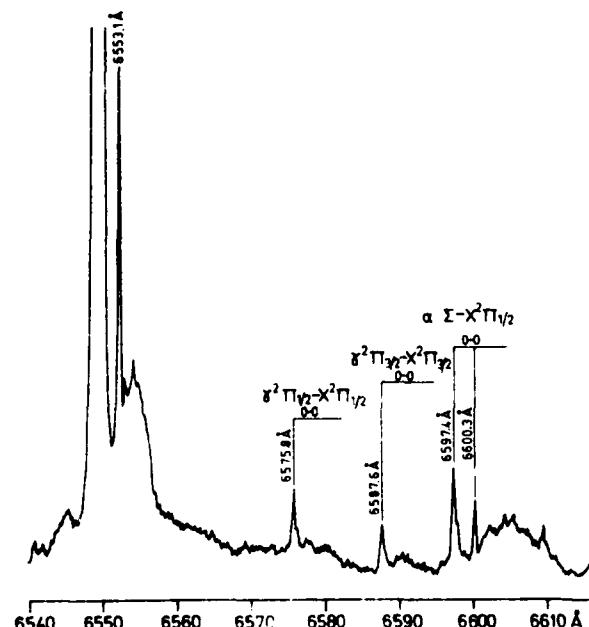
Fig. 3. Laser excitation spectrum of the $\gamma\,^2\Pi_i-X\,^2\Pi_i$ and $\alpha\Sigma-X\,^2\Pi_{1/2}$ band systems. Excitation into these states was monitored by the collisional transfer into the $A'\,^2\Sigma$ state. The monochromator was held fixed at 6429.7 Å which is the wavelength of the Q, head of the $A'\,^2\Sigma-X\,^2\Pi_{3/2}$ transition.
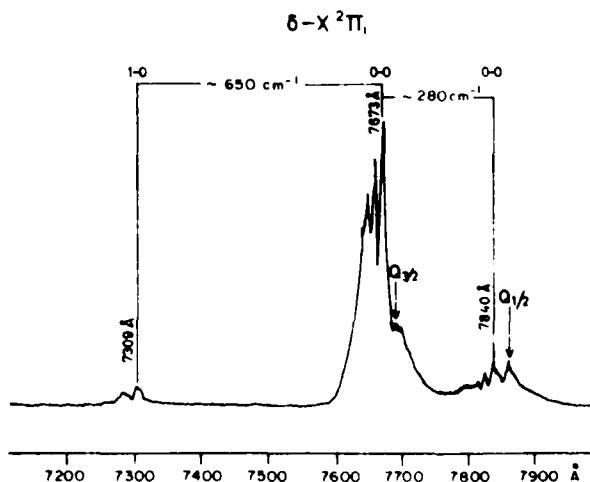
Fig. 4. Wavelength resolved laser induced fluorescence (uncorrected for spectrometer response). The upper state is populated by relaxation from the $A\,^2\Sigma$ state. Two band sequences, separated by approximately 280 cm^{-1}, are observed. The band system is interpreted as a $^2\Sigma-X\,^2\Pi_i$ transition, called here $\delta\,^2\Sigma-X\,^2\Pi_i$. The peak marked $Q_{1/2}$ is the Q head in the $\delta-X\,^2\Pi_{1/2}$ sub-band, the feature marked $Q_{3/2}$ is probably the Q head in the $\delta-X\,^2\Pi_{3/2}$ sub-band.

606   O. Appelblad, A. Lagerqvist, I. Renhorn and R. W. Field

Table I. Band heads of observed CuO bands in the red region

Transition	v' v''	Branch	(Å)	(cm⁻¹)	Rel.
$A^2\Sigma - X^2\Pi_{1/2}$	0-1	Q_2	6408.6	15 599.7	[25]
	1-2	Q_2	6403.9	15 611.1	[25]
	2-3	Q_2	6401.2	15 617.8	[25]
$A'^2\Sigma - X^2\Pi_{3/2}$	0-0	Q_1	6429.7	15 548.5	[16]
	0-0	$^SR_{21}$	6436.3	15 532.6	[16]
	1-1	Q_1	6440.6	15 522.1	This work
	1-1	$^SR_{21}$	6447.1	15 506.6	This work
$A'^2\Sigma - X^2\Pi_{1/2}$	0-0	$^PQ_{12}$	6546.3	15 271.6	[16]
	0-0	R_2	6553.1	15 255.7	[16]
	1-1	$^PQ_{12}$	6556.0	15 249.0	[16]
	1-1	R_2	6562.7	15 233.4	This work
	2-2	$^PQ_{12}$	6565.8	15 226.2	[16]
	2-2	R_2	6573.2	15 209.1	This work
$\alpha \Sigma - X^2\Pi_{3/2}$	0-0	R ?	6478.8	15 430.7	This work
	0-0	Q ?	6481.6	15 424.0	This work
$\alpha \Sigma - X^2\Pi_{1/2}$	0-0	R ?	6597.4	15 153.3	This work
	0-0	Q ?	6600.3	15 146.6	This work
$\beta^2\Delta_{3/2} - X^2\Pi_{1/2}$	0-0	R	6493.4	15 396.0	[17]
	1-1	R	6503.0	15 373.3	This work
$\beta^2\Delta_{5/2} - X^2\Pi_{3/2}$	0-0	R	6522.1	15 328.3	[17]
	1-1	R	6532.3	15 304.3	[17]
$\beta^2\Delta_{3/2} - X^2\Pi_{3/2}$	0-0	R	6378.9	15 672.3	This work
$\gamma^2\Pi_{1/2} - X^2\Pi_{1/2}$	0-0	R	6575.8	15 203.1	This work
$\gamma^2\Pi_{3/2} - X^2\Pi_{3/2}$	0-0	R	6587.6	15 175.8	This work
$\gamma^2\Pi_{1/2} - X^2\Pi_{3/2}$	0-0	R	6458.2	15 479.8	This work
$\delta^2\Sigma - X^2\Pi_{3/2}$	0-0	R ?	7673	13 029	This work
	1-1	R ?	7662	13 048	This work
	2-2	R ?	7653	13 063	This work
	3-3	R ?	7646	13 075	This work
	1-0	R ?	7309	13 678	This work
$\delta^2\Sigma - X^2\Pi_{1/2}$	0-0	R ?	7840	12 752	This work
	0-0	Q ?	7866	12 709	This work

Table II. Approximate T_0 values of new low lying CuO electronic states as estimated from the band heads

State	T_0 (cm⁻¹)
$\alpha\Sigma$	15 424
$\gamma^2\Pi_{1/2}$	15 470
$\gamma^2\Pi_{3/2}$	15 166
$\delta^2\Sigma$	12 986

similar structure, the observable perturbation matrix element is a good sample of the purely electronic factor, the vibrational factor being approximately unity. For states of similar structure, $\Delta v = 0$ perturbation effects are usually manifested only as intensity borrowing and interference effects. The perturbation matrix elements derived from intensity effects indicate whether the two interacting states differ by a single Cu-centered orbital.

5.1.3. *Kronig symmetry of lowest lying Σ states.* It is not possible to experimentally establish the e/f symmetry of a level or whether a state is Σ^+ or Σ^-. Configurational predictions of the symmetry of the lowest $^2\Sigma$ and $^4\Sigma$ states and the relative abundance of $^2\Sigma^+$ vs. $^2\Sigma^-$ states will ultimately resolve the e/f ambiguity and, indirectly, identify plausible low lying electronic configurations.

5.1.4. *Intrinsic transition strengths.* Once intensity borrowing effects are understood, relative deperturbed oscillator strengths for many electronic transitions may be estimated and used to group states into those belonging to configurations differing only by one Cu or O centered orbital and those differing from the $X^2\Pi_i$ state by two orbital excitations.

5.1.5. *Hyperfine structure.* Cu has $I = 3/2$. Thus a state with a half filled Cu-centered σ orbital will exhibit large Fermi-contact hyperfine splittings. Experiments, capable of resolving hfs in CuO, are now in progress.

Approximate T_0 values for the new states, as determined from the band heads are given in Table II.

The vibrational intervals of the new states have been calculated from the observed band heads and the known vibrational spacings of the $X^2\Pi_i$ state. Band heads have been determined to ± 1 cm⁻¹ for the $\delta-X$ system and to ± 0.3 cm⁻¹ for the other systems. Vibrational intervals are listed in Table III. The following approximate values of the equilibrium vibrational constants for the $\delta^2\Sigma$ state are:

$$\omega_e = 661 \, (1) \, \text{cm}^{-1}$$

$$\omega_e x_e = 5.7 \, (5) \, \text{cm}^{-1}$$

The spin-orbit constants of the $\beta^2\Delta_i$ and $\gamma^2\Pi_i$ states are approximately -172 ± 1 cm⁻¹ and -304 ± 1 cm⁻¹ respectively.

5.2. *Diagonal spin-orbit*

If the $3d$ shell in Cu is closed, we expect spin-orbit constants typical for oxygen. This prediction originates from consideration of one-electron matrix elements in single configurational wavefunctions [26 28]. The a_z values, discussed in, e.g. [27], for the elements O, S and Se are given in Table IV [29]. The corresponding spin-orbit parameter in the Cu shell is 817 cm⁻¹ [30]. The observed spin orbit constants A_Π of the $X^2\Pi_i$ state for the molecules CuO, CuS and CuSe are -277, -433 and -1591 cm⁻¹ respectively [31]. For this reason the following configuration may be suggested for the ground state $X^2\Pi_i$ of CuO:

$$(8\sigma^2 \, 3\pi^4 \, 1\delta^4 \, 9\sigma^2 \, 4\pi^3) \, X^2\Pi_i,$$

where the molecular orbitals 8σ, 3π and 1δ are centered pri-

5. Discussion

The electronic configurations of the low lying states of the group II B oxides are still under debate. Here we will summarize the various types of information that will ultimately provide the key to a simple configurational picture of the electronic structure of CuO. The most important of these are:

5.1.1. *Spin-orbit splittings of Π and Δ states.* These indicate the state of occupancy of π or δ orbitals and whether the incompletely filled orbital is located primarily on Cu or O.

5.1.2. *Spin orbit interactions between states.* Whenever there is a $\Delta v = 0$ interaction between two electronic states of

Table III. Vibrational intervals of the states A', β and δ

State	$v' + \frac{1}{2}$	$\Delta G^a_{v'+\frac{1}{2}}$ cm⁻¹	References
$A'^2\Sigma$	1/2	605.0	[16]
	3/2	596.0	[16]
$\beta^2\Delta_{5/2}$	1/2	607.3	[17]
$\beta^2\Delta_{3/2}$	1/2	604(1)	This work
$\delta^2\Sigma$	1/2	649.4(7)	This work
	3/2	637.8(7)	This work
	5/2	626.6(7)	This work

^{a} The number in parentheses is the estimated uncertainty in the last digit.

Table IV. *Atomic spin-orbit parameters*

Atom	a_z (cm^{-1})
O	151
O	121
S	382
S	325
Se	1690
Se	1527
Cu	817
Cu*	828
Ag	1789
Ag*	1830

Ref. [29, 30]

marily on copper and 9σ and 4π on oxygen. This configuration correlates with the separated ions $Cu^+(^1S)$ and $O^-(^2P)$. If we compare the spin-orbit constant A_{11} of the isovalent molecules CuO, CuS and CuSe with the spin-orbit parameter a_z of the atomic negative ions O^-, S^- and Se^-, a systematic deviation is observable. The spin-orbit constant is larger and increases slower in the molecule than in the comparable group VI ion. Therefore it seems likely that the Cu $3d$ shell is polarized in the ground state. This polarization is expected to decrease as one goes from CuO to CuSe thus explaining the slower increase in A_{11} with respect to a_z. A further indication that this might be the case is the magnitude of the spin-orbit constant for the ground state of AgO which is about -400 cm^{-1} [32]. AgO should have a larger A_{11} than CuO because the polarization and the a_z value for the Ag $4d$ shell are larger than for Cu $3d$.

5.3. *Off-diagonal spin-orbit effects*

It is possible to label the electronic states following a Hund's case 'a' nomenclature. However, the mutual interaction between different electronic states is quite large, which gives rise to numerous perturbations and intensity anomalies. Such have been found for example in the $A\,^2\Sigma-X\,^2\Pi_i$, $C\,^2\Pi_r-X\,^2\Pi_i$, and $D\,^2\Delta_i-X\,^2\Pi_i$ systems [15]. Since the $A-X$ transition moment is larger than the $C-X$ transition moment, a small mixing between the A and C states causes large intensity anomalies in the $C\,^2\Pi_{1/2}-X\,^2\Pi_i$ transition but not in the $A-X$ transition. In the $C\,^2\Pi_{1/2}-X\,^2\Pi_{1/2}$ transition, the R_e and P_f branches are strong while the R_f and P_e branches are very weak. The absolute e/f labeling is not known but we follow here the assignment given in [15]. In the $C\,^2\Pi_{1/2}-X\,^2\Pi_{3/2}$ transition, only the Q

Table V. *Transition strengths of band system involving low lying electronic states of the CuO molecule relative to the $A\,^2\Sigma-X\,^2\Pi_i$ transition*

Transition	Relative transition strength[a]
$A\,^2\Sigma-X\,^2\Pi_i$	100
$A'\,^2\Sigma-X\,^2\Pi_i$	6
$\beta\,^2\Delta-X\,^2\Pi_i$	0.5
$\alpha\,\Sigma-X\,^2\Pi_i$	2.5
$\gamma\,^2\Pi_r-X\,^2\Pi_i$	1.1
$\delta\,^2\Sigma-X\,^2\Pi_{3/2}$	~0.25
$\delta\,^2\Sigma-X\,^2\Pi_{1/2}$	~0.05

[a] Intensities are recorded under identical experimental conditions. Corrections are made for the wavelength dependent response of the photomultiplier and the v^4 factor.

branches have been observed. The unusually large intensity of the normally weak Q branches in a $\Pi-\Pi$ transition is due to the intensity borrowed from the $A\,^2\Sigma-X\,^2\Pi$ system. Similarly, the nominally forbidden $D\,^2\Delta_{3/2}-X\,^2\Pi_{1/2}$ sub-band is present because it borrows intensity through an interaction of $D\,^2\Delta_{3/2}$ with the $C\,^2\Pi_{3/2}$ state.

The appearance of the $A'\,^2\Sigma$, $\beta\,^2\Delta_i$ and $\gamma\,^2\Pi$ states is very similar to that of the A, C and D states. The $A'\,^2\Sigma-X\,^2\Pi_i$ transition is more intense than the $\beta\,^2\Delta_i-X\,^2\Pi_i$ and $\gamma\,^2\Pi_{1/2}-X\,^2\Pi_i$ transitions. Because of the mixing between the $A'\,^2\Sigma$ and $\gamma\,^2\Pi_{1/2}$ states, the $\gamma\,^2\Pi_{1/2}-X\,^2\Pi_{3/2}$ transition is present. From this fact we can predict interference derived $R \to P$ intensity anomalies in the $\gamma\,^2\Pi_{1/2}-X\,^2\Pi_{1/2}$ transition similar to those observed in the $C\,^2\Pi_{1/2}-X\,^2\Pi_{1/2}$ transition [15]. The observed intensity of the $\beta\,^2\Delta_{3/2}-X\,^2\Pi_{3/2}$ transition is likely to be the result of an interaction between the $\beta\,^2\Delta_{3/2}$ and $\gamma\,^2\Pi_{3/2}$ states.

Adopting the unique perturber approximation, some factors of two estimates of the mutual interaction strength among the low lying states can be carried through from observed intensity ratios. If our observation of the intercombination transition $\gamma\,^2\Pi_{1/2}-X\,^2\Pi_{3/2}$ is due to intensity borrowing from the $A'\,^2\Sigma-X\,^2\Pi_i$ transition moment, then the $A'\,^2\Sigma \sim \gamma\,^2\Pi_{1/2}$ interaction can be estimated. The intensity ratio between $I(A'-X)$ and $I(\gamma_{1/2}-X_{3/2})$ is about $20:1$. Thus, the $A'\,^2\Sigma$ character mixed into the $\gamma\,^2\Pi_{1/2}$ state is approximately 5 per cent. This character is also given by $\sin^2\theta$, where $\sin\theta$ is the mixing coefficient and,

$$\tan 2\theta = \frac{|H_{A'\gamma}|}{\sqrt{\left[\left(\frac{\Delta T_{A'\gamma}}{2}\right)^2 - H_{A'\gamma}^2\right]^{1/2}}}$$

$\Delta T_{A'\gamma}$ is the observed term value difference between the $A'\,^2\Sigma$ and $\gamma\,^2\Pi_{1/2}$ states (~ 54 cm^{-1}). From these observations the perturbation matrix element $|H_{A'\gamma}|$ can be calculated. If the vibrational overlap factor is ~ 1, then the electronic part of the spin-orbit interaction between the $A'\,^2\Sigma$ and $\gamma\,^2\Pi$ states has the rather small value of 12 cm^{-1}. This indicates an "orbitally" forbidden interaction. By this we mean that the two configurations differ by more than one spin-orbital or that the interacting orbitals are located on different atomic centers. We must reiterate that these are only factor of two estimates.

5.4. *Kronig symmetry*

We have, so far, avoided discussing the Kronig symmetry of the $^2\Sigma$ states. The e/f parities of a state are generally settled when theoretical predictions and spectroscopic determinations agree. As no such agreement has yet been obtained for CuO, there is no possibility of deciding the parity of observed states. For convenience, the chronologically first rotationally analyzed $^2\Sigma$ state, $A\,^2\Sigma$, was arbitrarily assigned as a $^2\Sigma^+$ state [11]. However, one could argue that, similarly with the group I A oxides, there should be a low lying $^2\Sigma^+$ state in more or less "pure precession" with the $X\,^2\Pi_i$ state. For KO, RbO and CsO there is theoretical [33] and experimental [34] evidence that a $^2\Sigma^+$ state is the ground state with a very low lying $^2\Pi$ state close by. For NaO there is theoretical evidence of a $^2\Pi$ ground state with a close lying $^2\Sigma^+$ state [33, 35]. The Λ-type doubling of the $X\,^2\Pi_i$ ground state of CuO indicates a close lying $^2\Sigma$ state. The strong vibrational variation of the spin-orbit constant A_v is another indication that such is the case. Nevertheless, it is surprising that transitions involving this

missing state have not appeared in the laser excitation or fluorescence spectra. It is not possible that either the $\delta^2\Sigma$ or $\alpha\Sigma$ state is this missing state.

An intensity anomaly, of a type not previously noted, is observed in the $\delta^2\Sigma-X^2\Pi_i$ band system in which the two sub-bands have different intensities. If this anomaly has its origin in the $A' \sim \delta$ interaction, we can estimate this interaction matrix element from observed intensities. From the laser induced fluorescence experiments, the ratio between the $I(A' - X)$ and $I(\delta - X)$ intensities is about 50:1. This ratio is uncertain by a factor of two but can still provide useful estimates of the interaction strength. From the observed intensity ratio, the ratio between the transition moments is obtained. The result is approximately $\mu_{A'X}/\mu_{\delta X} \sim 5:1$. The intensity ratio between the two sub-bands in the $\delta-X$ transition is about 5:1. As shown in [36], this ratio can be used to estimate $A'^2\Sigma \sim \delta^2\Sigma$ mixing. If this interpretation is correct, the $A'^2\Sigma$ and $\delta^2\Sigma$ states have opposite Kronig symmetries. With the values given above, this mixing coefficient will be $\sin\theta = 0.076$ and the perturbation matrix element $|H_{A'\delta}| \sim 190\,\mathrm{cm}^{-1}$. Again, since this is a $\Delta v = 0$ interaction between states of nearly identical potentials, the vibrational factor is ~ 1 and the electronic part of this spin-orbit interaction is large enough to be "orbitally" allowed. By "orbitally" allowed means that the two configurations differ by one spin-orbital. The two connected orbitals are also mainly located on the same atom.

5.5. Intrinsic transition strengths

The most intense band system observed so far in CuO is the $A^2\Sigma-X^2\Pi_i$ system. Parts of this transition strength are distributed among neighbouring systems. This is manifested, e.g. as an intensity anomaly in the $C^2\Pi_r-X^2\Pi_i$ band system and may very well constitute a substantial part of the $A'^2\Sigma-X^2\Pi_i$ transition strength. We can list the transition strengths of the neighbouring band systems relative to the $A^2\Sigma-X^2\Pi_i$ system. The estimates are given in Table V.

6. Summary

Three new low lying states of CuO are recognized, $\alpha\Sigma$, $\gamma^2\Pi_i$, and $\delta^2\Sigma$. Even without a full rotational analysis, considerable information is derived relevant to the nature of the lowest lying electronic configurations of CuO. It is very tempting to assign the $A'^2\Sigma$, $\alpha^4\Sigma$, $\beta^2\Delta$ and $\delta^2\Sigma$ to the configuration:

$$(8\sigma^2, 3\pi^4 1\delta^4 9\sigma^2 4\pi^2 10\sigma)$$

This configuration is in agreement with the $A'^2\Sigma \sim \delta^2\Sigma$ interaction discussed above. However, final configurational assignments will be premature until rotational analyses of the $\alpha\Sigma$, $\gamma^2\Pi_i$ and $\delta^2\Sigma$ states have been carried out. This will determine whether the $\gamma^2\Pi_i$ and $\delta^2\Sigma$ states are involved in pure precession relationships with other known or still unknown states and also if the $\alpha\Sigma$ state is a quartet state or not. If this information is combined with information about the hyperfine structure of the different states, configurational assignments and the Kronig symmetries of the different Σ states may be settled.

Bands remain in the visible region of the CuO spectrum, particularly in the violet region, which have not been vibrationally and rotationally analyzed. Of even greater importance is the $\delta^2\Sigma-X^2\Pi$ near infrared band system, for which a rotational

analysis would clear up some crucial features of the electronic structure of CuO. Attempts to discover new states lying between the $\delta^2\Sigma$ and $X^2\Pi_i$ states and systematic examination of the hyperfine structure of low lying states will also be valuable.

References

1. Hertenstein, H., Z. Wiss. Photogr. 11, 199 (1912).
2. Mahanti, P. C., Nature 125, 819 (1930).
3. Loomis, F. W. and Watson, T. F., Phys. Rev. 48, 280 (1935).
4. Lejeune, J. M. and Rosen, B., Bull. Soc. Roy. Sci., Liege 14, 81 (1945).
5. Guntsch, A., Ark. Mat. Astr. Fys. A33, No. 2 (1946).
6. Antic-Jovanovic, A., Pešić, D. S. and Gaydon, G., Proc. Roy. Soc., London A307, 399 (1968).
7. Appelblad, O. and Lagerqvist, A., Physica Scripta 10, 307 (1974).
8. Antic-Jovanovic, A. and Pešić, D. S., J. Phys. B6, 2473 (1973).
9. Lagerqvist, A. and Uhler, U., Z. Naturforsch. 22B, 551 (1967).
10. Appelblad, O., Lagerqvist, A. and Lyyra, M., Physica Scripta 20, 93 (1979).
11. Appelblad, O. and Lagerqvist, A., J. Mol. Spectrosc. 48, 607 (1973).
12. Appelblad, O. and Lagerqvist, A., Can. J. Phys. 53, 2221 (1975).
13. Appelblad, O. and Lagerqvist, A., Physica Scripta 13, 275 (1976).
14. Lefebvre, Y., Pinchemel, B. and Bacis, R., Can. J. Phys. 54, 735 (1976).
15. Appelblad, O., Lagerqvist, A., Lefebvre, Y., Pinchemel, B. and Schamps, J., Physica Scripta 18, 125 (1978).
16. Lefebvre, Y., Pinchemel, B. and Schamps, J., J. Mol. Spectrosc. 68, 81 (1977).
17. Pinchemel, B., Lefebvre, Y. and Schamps, J., J. Phys. B: Atom. Molec. Phys. 10, 3215 (1977).
18. Appelblad, O., Lagerqvist, A. and Lyyra, M., Physica Scripta 18, 137 (1978).
19. West, J. B., Bradford, R. S., Eversole, J. D. and Jones, C. R., Rev. Sci. Instrum. 46, 164 (1975).
20. Field, R. W., English, A. D., Tanaka, T., Harris, D. O. and Jennings, D. A., J. Chem. Phys. 59, 2191 (1973).
21. Field, R. W., Capelle, G. A. and Revelli, M. A., J. Chem. Phys. 63, 3228 (1975).
22. Jones, C. R. and Broida, H. P., J. Chem. Phys. 60, 4369 (1974).
23. Gottscho, R. A., Koffend, J. B., Field, R. W. and Lombardi, J. R., J. Chem. Phys. 68, 4110 (1978).
24. Shirk, J. S. and Bass, A. M., J. Chem. Phys. 52, 1894 (1970).
25. Appelblad, O., (unpublished data).
26. Field, R. W., Wicke, B. G., Simmons, J. D. and Tilford, S. G., J. Mol. Spectrosc. 47, 194 (1973).
27. Field, R. W., Lagerqvist, A. and Renhorn, I., Physica Scripta 14, 298 (1976).
28. Field, R. W., Lagerqvist, A. and Renhorn, I., J. Chem. Phys. 66, 868 (1977).
29. Hotop, H., Patterson, T. A. and Lineberger, W. C., Phys. Rev. A8, 762 (1973).
30. Moore, C. E., Atomic Energy Levels, Natl. Bur. Std. Circ. No. 467, U.S. GPO, Washington, D.C. (1952).
31. Huber, K. P. and Herzberg, G., Molecular Spectra and Molecular Structure, Van Nostrand Reinhold Company (1979).
32. Griffiths, M. J. and Barrow, R. F., J. Phys. B: Atom. Molec. Phys. 10, 925 (1977).
33. So, S. P. and Richards, W. G., Chem. Phys. Lett. 32, 227 (1975).
34. Lindsay, D. M., Herschbach, D. R. and Kwiram, A. L., J. Chem. Phys. 60, 315 (1974).
35. O'Hare, P. A. G. and Wahl, A. C., J. Chem. Phys. 56, 4516 (1972).
36. Renhorn, I. Mol. Phys., (in press).

Rotational and Hyperfine Analysis of the 0,0 Band of the PrO XX System

Michael Dulick, Robert W. Field
Massachusetts Institute of Technology
Spectroscopy Laboratory and the Department of Chemistry
Cambridge, Massachusetts 02139

J. Cl. Beaufils[1]
U.E.R. de Physique Fondamentale
Université de Lille
B.P. 36
59650 Villeneuve d'Ascq, France

<u>20</u> Pages

<u>5</u> Tables (10 pages)

<u>1</u> Figure

Table of Symbols

Δ   Cap. Greek delta

Σ   Cap. Greek sigma

Φ   Cap. Greek phi

Γ   Cap. Greek gamma

Ω   Cap. Greek omega

σ   l.c. Greek sigma

φ   l.c. Greek phi

δ   l.c. Greek delta

ν   l.c. Greek nu

α   l.c. Greek alpha

β   l.c. Greek beta

$B\ 0^+_u$ Cap. Roman B, half space, <u>zero</u>, superscript, subscript

Σ   large summation sign.

>   greater than

<   less than

ABSTRACT

The PrO XX 0-0 band is recorded at Doppler-limited resolution
by laser excitation spectroscopy with selective fluorescence detection.
The rotational and hyperfine structure of this $\Omega' = 5.5 - \Omega'' = 4.5$
band is reanalyzed. In addition, fluorescence spectra obtained
through excitation of selected rotational lines in the XX 0-0 band
and by the 529 nm Ar+ laser line have established an energy ordering
of four low-lying $\Omega = 4.5$ states and one $\Omega = 6.5$ state as well as ΔG ($\frac{1}{2}$)
values for the $\Omega = 6.5$ and the two lowest $\Omega = 4.5$ states. Principal
constants, in cm^{-1}, are (1σ uncertainties in parentheses, * indicates
constant held fixed):

	T_0	$\Delta G(\frac{1}{2})$	B_0
$\Omega' = 5.5$(System XXII)	18 944 (1)	——	0.356*
$\Omega' = 5.5$(System XX)	17 845.737 (1)	——	0.355 904 (23)
$\Omega'' = 4.5$	5 720.5 (10)	——	0.356 (7)
$\Omega'' = 6.5$	3 736.0 (10)	830.9 (6)	0.362 (7)
$\Omega'' = 4.5$	3 500.3 (3)	——	0.3556 (3)
$\Omega'' = 4.5$	1 936.7 (2)	833.0 (4)	0.3637 (2)
$\Omega'' = 4.5$(System XX and XXII)	0*	831.8 (4)	0.361 918 (22)

Hyperfine constants, in cm^{-1}, for the lowest of the above $\Omega' = 5.5$
and $\Omega'' = 4.5$ states (System XX, $v' = v'' = 0$) are:

$\Omega' = 5.5$ $d' = 0.1328$ (15) $d'_J = 0*$

$\Omega'' = 4.5$ $d'' = 0.2816$ (17) $d''_J = 6.67$ (54) $\times 10^{-5}$.

Excitation spectra, to be reported separately, have shown that the
529 nm Ar^+ laser line excites System XXII 0-0 P(34.5).

I.   INTRODUCTION

The electronic spectrum of PrO was classified by Shenyavskaya et al. (1) into 22 systems spanning the wavelength region 5000-11200 Å. They reported vibrational constants for the upper and lower electronic states of these systems obtained from analysis of bandheads as well as rotational constants from rotational analyses of the VII system 0-0 , 0-1, and 1-0 bands and the 0-0 band of the X system. That work was followed by a rotational reanalysis by Delaval et al. (2,3) of systems VII and X. More recently, rotational and hyperfine analyses of the XVII and XX systems were reported by Beaufils et al. (4). Recently, the present authors (5) proved that the analysis of the XVII system hyperfine structure (4) was incorrect.

The lowest J" lines of the VII and X systems were too weak to be observed by Delaval (2,3), thus his Ω',Ω'' assignments were speculative. He suggested that the lower states of these systems involved the spin components of a $\sigma^2\phi$ $^2\Phi$ ground state, analogous to the $\sigma^2\delta$ $^2\Delta$ electronic ground state of TaO. Beaufils et al. (4) observed the first R lines of the XVII and XX systems and assigned them as J" = 3.5 and 4.5, respectively. Based on the good agreement between lower state combination differences of the XVII and XX systems with those of the VII and X systems, respectively, and the erroneous hyperfine analysis, Beaufils et al. (4) concluded that these two pairs of systems orginated from a $^2\Gamma$ ground state.

In order to obtain a better understanding of the PrO electronic structure, we have reanalyzed the rotational and hyperfine structure of the XVII and XX 0-0 bands and analyzed the XXI 0-0 and 0-1 bands

recorded at Doppler-limited resolution by cw, 1 MHz bandwidth laser excitation spectroscopy with selective-fluorescence-detection (which eliminates inter-band blends). In addition, spectra of the fluorescence arising from selected lines in systems XVII, XX, and XXI and from an electronic transition excited by the 529 nm line of an argon ion laser were analyzed in order to energy-order the numerous low-lying states of PrO. These results are presented in two papers.

This paper describes the rotational and hyperfine structure of the system XX 0-0 band and the rovibronic structure of five low-lying states characterized by fluorescence excited <u>via</u> two electronic transitions. These transitions, system XX and another (possibly system XXII)[2] excited by the 529 nm Ar+ laser line, are shown to share a common $\Omega'' = 4.5$ lower state. The following paper describes systems XVII and XXI and a new system which involves excitation from the lower state of system XXI to the upper state of system XVII.

II. DESCRIPTION OF EXCITATION AND FLUORESCENCE SPECTRA

The red-degraded XX 0-0 band with bandhead at 559.66 nm consists of P, Q, and R branches. The Q branch is the most intense, followed by a weaker R branch and an anomalously weak P branch. From our rotational analysis, we have established that the first lines of the R and P branches are R(4.5) and P(6.5). Thus, the XX system is $\Delta\Omega = + 1$ with $\Omega" = 4.5$ and $\Omega' = 5.5$.

$J"< 30.5$ rotational lines are broader than their expected Doppler width owing to hyperfine structure. At low J (for example, $J" < 17.5$ in the R branch), where the hyperfine structure is resolvable under Doppler-limited conditions, each rotational line is composed of six main hyperfine lines. Natural praseodymium consists of one isotope, ^{141}Pr, with a nuclear spin of 2.5, a large magnetic moment of + 3.4 nuclear magnetons, and a quadrupole moment of + 1.2 x 10^{-24} cm^2 (6). A minimum of six, $|J + I|$ to $|J - I|$, hyperfine lines are expected for each rotational line, corresponding to the strongest ($\Delta F = \Delta J$) transitions. Additional weak hyperfine lines are observed in the R branch. In particular, for the R(4.5) transition, where the hyperfine lines are spread over a 0.75 cm^{-1} interval, four weak lines are present in addition to the six main lines. For R(5.5) to R(14.5) only one weak extra hyperfine line is observed. An analysis of the low-J Q lines was impossible due to extensive blending of hyperfine lines between consecutive Q branch transitions. The intensity pattern for the hyperfine lines in the P and R branches is consistent with that predicted for case a_β (or c_β) coupling (7).

It was observed that hyperfine splittings for P lines were considerably
smaller than splittings for R lines of the same upper or lower J.
Fully resolved hyperfine splittings were observed in the R and P branches
up to R(17.5) and P(9.5). The shading of the hyperfine lines within each
rotational line (F_{min} to F_{max}) is to longer wavelength for both branches.

The XX 0-0 band exhibits several perturbations, all of the upper
state. Perturbation effects first become noticable at $J' = 35.5$ where
the main line (hfs no longer resolvable) appears to begin to split into
two components. This pattern is consistent with a perturbation by a
state possessing significant Ω-doubling, quite surprising when one considers
that the perturber must have $\Omega \geq 4.5$. A more detailed discussion of this
and other perturbations must await further Doppler-free experiments
and more complete knowledge of the electronic level diagram of PrO.

The spectrum of fluorescence which results from excitation in the
XX 0-0 band contains four bands to the red and none to the blue of
the laser-excited band. These bands are located near 587, 628, 662,
and 696 nm. The fluorescence excited by the Ar^+ laser 529 nm line contains
five bands to the red and none to the blue of the laser excitation band.
Their wavelengths are 588, 647, 657, 695, and 756 nm.

III. EXPERIMENTAL

PrO is produced in a Broida-type oven ([8]), modified for high temperature use, by heating Pr_6O_{11} with a trace of Pr metal to 1300-1400°C in a graphite crucible (Ultracarbon UPG Grade UF-4S with PT-101 Pyrolytic Graphite Coating). The vaporized PrO is entrained in flowing argon at typical operating pressures of 1-3 torr. High resolution excitation spectra (Doppler-limited resolution, 0.025 cm^{-1} FWHM) are obtained by scanning a single-mode Coherent Model 599-21 dye laser (bandwidth < 1 MHz), operated with rhodamine 110 dye, over consecutive 1 cm^{-1} intervals and detecting fluorescence through a 1 meter Spex monochromator functioning as a narrow bandpass filter. The monochromator-selected spectral widths were 0.05 to 0.2 nm. The advantages of narrow-band fluorescence detection are discussed elsewhere ([9],[10]).

Fluorescent spectra were obtained by excitation of a selected, single rotational line with the frequency of the dye laser held fixed and by scanning the monochromator in second order (1200 grooves/mm, 1.2 μm blaze grating) with spectral slitwidths of 0.1 - 0.2 nm. Fluorescent spectra were calibrated ($\pm$ 0.3 cm^{-1}) with respect to neon and argon atomic lines, while excitation spectra were calibrated ($\pm$ 0.003 cm^{-1} absolute) with respect to I_2 B 0_u^+ - $X^1\Sigma^+$ lines ([11]) and a 300 MHz free spectral range, semi-confocal Fabry-Perot ($\pm$ 0.001 cm^{-1} relative).

IV. RESULTS

A. XX 0-0   Band Rotational Analysis

The P, Q, and R branch rotational lines for the 0-0   band
of the XX system, recorded by selective fluorescence detection, are
listed in Table 1. The absolute accuracy of the line positions for most
cases is $\pm$ 0.003 cm^{-1}. The exceptions are the P lines for $6.5 \leq J'' \leq 10.5$
where the accuracy is reduced by as much as a factor of five. The lower
accuracy is the result of poor signal to noise, due to the weak intensity of these
lines and the 0.05 nm fluorescence-detection spectral bandwidth needed in order to
significantly reduce the intensity of strong Q lines which are present in the
same spectral region. Even with a 0.05 nm bandwidth, Q lines belonging to higher J''
were still present and blended with several hyperfine components of the
low-J P lines.

The rotational constants for the $\Omega' = 5.5$ and $\Omega'' = 4.5$ states were
obtained from a fit of energy levels using a weighted, nonlinear, least-
squares procedure. (The nonlinear capability is required only for analysis
of perturbations). For the $J'' < 20.5$ rotational lines of the P and R branches,
it was necessary to calculate rotational line centers using hyperfine
constants obtained from the hyperfine analysis (see Sec. IV.B). The
derived rotational constants for the upper and lower states are reported
in Table 2. The band origin reported in Table 2 is defined with respect to the
equation,

$$\nu(J) = \nu_{00} + B'[J'(J'+1) - \Omega'^2] - B''[J''(J''+1) - \Omega''^2]$$
$$-D'[J'(J'+1)]^2 + D''[J''(J''+1)]^2 , \qquad [1]$$

as the extrapolated position of the nonexistent Q(0) line and differs from
the rotationless energy separation by $B'\Omega'^2 - B''\Omega''^2$.

B. Hyperfine Analysis

The qualitative appearance of the hyperfine structure leads
to the following conclusions:

1) Significant hyperfine splittings exist in <u>both</u> upper
   and lower electronic states,

2) The hyperfine structure is regular, i.e., $E(J,F) < E(J,F+1)$,

3) A larger hyperfine interaction exists in the lower
   state.

The spacings of hyperfine components within a rotational transition
were measured to a relative precision of ± 0.001 cm^{-1}. A list of
measured hyperfine lines along with observed (fitted) and calculated
differences is presented in Table 3.

The hyperfine splittings and intensities of the XX 0-0 band
are well represented by the a_β (or c_β) coupling case. Case a_β matrix
elements were obtained from Frosch and Foley (12). The hyperfine energy
level expression for an electronic state is

$$E(F,J) = [d-d_J J(J+1)] \frac{\Omega}{2J(J+1)} [F(F+1)-J(J+1)-I(I+1)]$$

$$+ \sum_{J*} \frac{|<F,J| H^{hfs} |F,J*>|^2}{B[J(J+1) - J*(J*+1)]}$$

[2]

where the first term represents the $\Delta F=\Delta J=0$ matrix element of the hyperfine

Hamiltonian and the second term is the second order perturbation theory correction which arises from $\Delta J = \pm 1$ matrix elements.

The hyperfine constant, d, and its centrifugal distortion correction, d_J, for both electronic states were obtained by simultaneously fitting differences between $\Delta J = \Delta F = +1$ and -1 hyperfine lines of the R_F^r and P_F^p lines ($\Delta J_F^{\Delta F}$) to the expressions

$$R_{F''+1}^r(J'') - R_{F''}^r(J'') = [E_{hfs}'(F''+2,J''+1) - E_{hfs}'(F''+1,J''+1] - [E_{hfs}''(F''+1,J'') - E_{hfs}''(F'',J'')] \quad [3]$$

and

$$P_{F''-1}^p(J'') - P_{F''}^p(J'') = [E_{hfs}'(F''-2,J''-1) - E_{hfs}'(F''-1,J''-1] - [E_{hfs}''F''-1,J'') - E_{hfs}''(F'',J'')] \quad [4]$$

using a nonlinear least-squares procedure. Because the rotational constants for the upper and lower electronic states are incorporated in the hyperfine energy level expression, it was necessary to use an iterative method to fit the rotational and hyperfine energy levels. This procedure involved: (1) a preliminary fit of the hyperfine splittings ignoring off-diagonal corrections; (2) rotational line centers were calculated from approximate hyperfine constants thus obtained using

$$\nu(J) = \frac{1}{6} \sum_{J''-2.5}^{J''+2.5} [\nu(F',J' + F'',J'') - E_{hfs}'(F',J') + E_{hfs}''(F'',J'')] \quad [5]$$

with $J' = J'' + 1$, $F' = F'' + 1$ or $J' = J'' - 1$, $F' = F'' - 1$ for the R or P branches, respectively, where off-diagonal corrections and $2F'' + 1$

statistical weights are ignored; (3) initial rotational constants were
obtained by including low-J rotational line centers as well as hyperfine-
blended higher-J lines in the fit; (4) these preliminary rotational
and hyperfine constants were then input as initial guesses for the nonlinear
fit to expressions 3 and 4 in which off-diagonal corrections were explicitly
included. Refitting the observed lines to expressions 3 and 4 provided
better estimates for the rotational line centers, especially for R(4.5)
to R(6.5). The rotational lines were then refit using these improved
line centers. The process was repeated until the change in hyperfine
and rotational constants between iterations was less than 1 part in 10^4.
A maximum of only two iteration cycles (excluding the initial fit to
obtain preliminary constants) was necessary to satisfy the convergence
criterion.

A least squares fit, incorporating quadrupole interaction terms for both
upper and lower electronic states (13), was performed, but the quadrupole
constants were statistically undetermined. In addition, centrifugal distortion
corrections for d' and d" were included in the hyperfine fit, but the
d' distortion constant was also statistically undetermined. In
contrast, inclusion of the distortion constant for d" reduced the
variance of the hyperfine fit by almost an order of magnitude and elimin-
ated systematic deviations in the residuals between low and high J
hyperfine splittings. Hyperfine constants d', d", and d''_J are presented
in Table 2.

The weak hyperfine lines observed in the R branch were found to
be $\Delta F = 0$ transitions when their positions relative to the parent $\Delta F = +1$

transitions were predicted using the hyperfine constants in Table 2. Differences between observed and calculated values for the five $\Delta F = 0$ hyperfine components of the R(4.5) line are listed in Table 4. The intensity ratio observed between the $\Delta F = + 1$ and $\Delta F = 0$ transitions with the same lower F" level, compared to the ratios calculated using the relations derived by Femenias et al. (14), indicate that the $\Delta F = 0$ transitions are more intense than expected. Such anomalous intensities could result from interaction between near degenerate electronic states. For J" > 5.5, the $\Delta F = 0$ transitions are buried under stronger $\Delta F = + 1$ transitions, except for the transition corresponding to F''_{max}.

C. Analysis of Fluorescence Spectra

Rotational numbering of lines in the fluorescence from the upper level of the XX 0-0 band near 560 nm was established from prior knowledge of the J' value of the selectively excited rotational line in the high resolution excitation spectrum. In all cases, either a P or Q excitation line was chosen. The rotational constants for the lower electronic states were obtained by fitting the rotational energy levels using a weighted least-squares procedure in which the upper state constants were held fixed at the values for the XX 0-0 band. Because rotational lines in the fluorescence spectra could be measured to an accuracy no better than $\pm$ 0.3 cm^{-1}, centrifugal distortion constants were not determined. They were fixed to the value of D''_0 of the XX 0-0 band.

All fluorescent bands (587, 628, 662, and 696 nm) contained a strong Q branch and weaker P and R branches, with the R branch more intense than the P branch. Therefore, all of the lower states were assigned as $\Omega'' = 4.5$. These relative intensity-based Ω-assignments must be regarded as preliminary, since a $\Delta\Omega = \pm 1$ perturbation in either the upper or lower state could result in misleading intensities and incorrect assignments.

The 587 nm band is the 0-1 band of the XX System. From this band, we obtain $\Delta G_{\frac{1}{2}} = 831.9$ cm^{-1}, which is in reasonable agreement with $\Delta G_{1/2}$ calculated using the Shenyavskaya et al. band head vibrational constants (1). The 628 and 662 nm bands are, respectively, the 0-0 and 0-1 bands of another $\Delta\Omega = +1$ transition. The 696 nm band is a 0-0 band of a third $\Delta\Omega = +1$ transition. Constants derived from analysis of the fluorescence spectrum are summarized by Table 5 and Figure 1.

Laser induced fluorescence was also excited by the 529 nm line of an Ar$^+$ ion laser. This laser line falls within the wavelength region of the Shenyavskaya et al. XXII 0-0 band (1). At this time[2] it is not possible to prove that the 529 nm line excites a line of the XXII 0-0. It is, however, possible to provide Ω, rotational, and vibrational assignments for the 529 nm excitation and to prove that it and System XX share a common lower state.

The 529 nm line excites a P(34.5) line (15). The J" value is determined from the observed lower state $\Delta_2 F(J'')$ combination difference and the B_0'' value determined from the XX 0-0 excitation spectrum.[3]

Proof that System XX 0-0 and the 529 nm excitation share an $\Omega'' = 4.5$, $v'' = 0$ level is obtained from differences between corresponding $P(J+1)$, $Q(J)$, and $R(J-1)$ lines in their respective fluorescence spectra. Five bands, 588, 647, 657, 695, and 756 nm, were observed to the red of the band containing the 529 nm laser excitation line. The separations of $Q(33.5)$ lines between 529, 588, and 647 nm bands match perfectly those of the $Q(33.5)$ lines of the XX 0-0 628, and 696 nm bands. The 529, 588, and 647 nm bands contain P, Q, and R lines with R stronger than P; thus $\Omega' = 5.5$. Vibrational assignments are based on the much greater intensity of $\Delta v = 0$ than $\Delta v = \pm 1$ bands for all known PrO electronic systems. The upper level of the 529 nm excitation is $v' = 0$ because the strongest fluorescence bands from it terminate in known $v'' = 0$ levels.

Two additional electronic transitions are present in the 529 nm excited fluorescence spectrum which were not observed for XX 0-0 excitation. We predict that the transitions to these two higher lying $\Omega'' = 6.5$ and $\Omega'' = 4.5$ states from the $\Omega' = 5.5$ state of the XX System will be reasonably strong, but the reason that they were not observed for the XX 0-0 excitation is that they lie beyond the red cut-off limit of our photomultiplier. As shown on Fig. 2, these transitions terminate on $\Omega'' = 4.5$ $v'' = 0$ and 6.5 $v'' = 0$ and 1 levels, all of which lie at higher energy than the highest level observed in the XX 0-0 excited fluorescence.

V. DISCUSSION

We conclude from the hyperfine analysis presented in this paper
that the analysis of tne hyperfine structure reported by Beaufils et al.
(4) for the XX system is incorrect. In the following paper we show
that the lower states of Systems XVII and XX, assigned by Beaufils
et al. (4) as components of a $^2\Gamma$ state, exhibit very similar vibration-
rotation constants but hyperfine d values of dramatically different
magnitudes. This suggests that these states are certainly not
components of any case 'a' doublet and probably do not even arise from
the same electronic configuration.

It is uncertain[2] whether the electronic transition $\Omega' = 5.5 \leftarrow \Omega'' = 4.5$
excited by the 529 nm argon ion line belongs to the XXII 0-0 band
identified by Shenyavskaya et al. (1). They observed only $\Delta v = 0$ sequence
bands for system XXII. Likewise, we observed only the $\Delta v = 0$ 0-0 band in
fluorescence from the 529 nm excited transition. Furthermore, only the $\Delta v = 0$ band
for the two low-lying $\Omega'' = 4.5$ states is observed. On the other hand,
the unusual absence of $\Delta v = -1$ bands in 529 nm excited fluorescence
contrasts with the situation for XX 0-0 excitation, from which 0-0
and 0-1 transitions are observed into the two lowest $\Omega'' = 4.5$ states.
This suggests that the upper electronic states of the 529 nm excitation
and System XXII are both shifted to slightly shorter R_e' than the
upper state of System XX and are identical.[2]

ACKNOWLEDGMENTS

REFERENCES

1. E.A. Shenyavskaya, I.V. Egorova, and V.N. Lupanov, J. Mol. Spectrosc. 47, 355-362 (1973).

2. J.M. Delaval, Thesis Université des Sciences et Techniques de Lille, 1977.

3. J.M. Delaval, J. Van Heems, and J. Cl. Beaufils, Canad. J. Spectrosc. 22, 117-120 (1977).

4. J. Cl. Beaufils, P. Carette, and J.M. Blondeau, J. Mol. Spectrosc. 77, 1-10 (1979).

5. M. Dulick, R.W. Field, and J. Cl. Beaufils, J. Mol. Spectrosc. 78, 333-334 (1979).

6. C.H. Townes and A.L. Schawlow, Microwave Spectroscopy, p. 647, McGraw-Hill, New York, 1955.

7. T.M. Dunn, " Nuclear Hyperfine Structure in the Electronic Spectra of Diatomic Molecules", in Molecular Spectroscopy: Modern Research, K. Narahari Rao and C. Weldon Mathews, Eds., Academic Press (1972), p. 231-257

8. J.B. West, R.S. Bradford, J.D. Eversole, and C.R. Jones, Rev. Sci. Instrum. 46, 164-168 (1975).

9. W. Demtröder, "Investigations of Small Molecules by Modern Spectroscopic Techniques", in Case Studies in Atomic Physics, M.R.C. McDowell, and E.W. McDaniels, Eds., Vol. 6 North-Holland, Amsterdam (1976).

10. M. Dulick, P.F. Bernath, and R.W Field, Can. J. Phys. 58, 703-712 (1980).

11. S. Gerstenkorn and P. Luc, Atlas du Spectre d'Absorption de la Molécule d'Iode CNRS, Paris, 1978.

12. R.A. Frosch and H.M. Foley, Phys. Rev. 88, 1337-1349 (1952).

13. C.H. Townes and A.L. Schawlow, Microwave Spectroscopy, p. 151, McGraw-Hill, New York, 1955.

14. J.L. Femenias, C. Athenour, and T.M. Dunn, J. Chem. Phys. $\underline{63}$, 2861-2868 (1975).

15. M. Dulick and R.W. Field, unpublished.
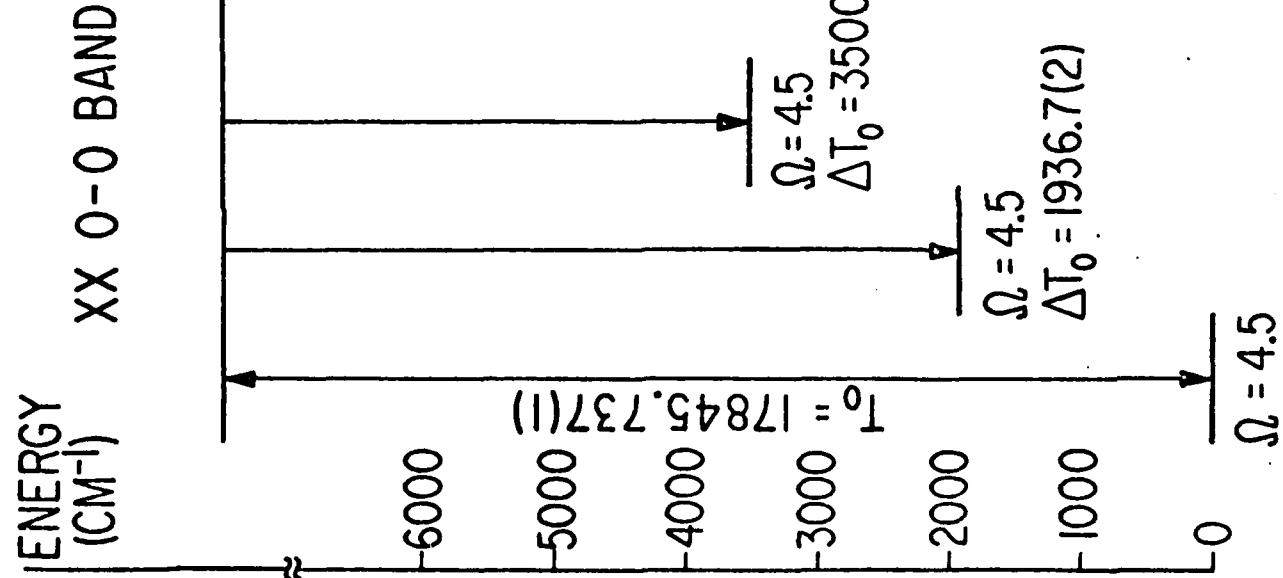
Footnotes

1. Visiting scientist at MIT.

2. Laser excitation spectra of the System XXII 0-0 band, recorded
    after this paper was completed, confirm that the Ar^+ laser
    529 nm line excites the P(34.5) line of this band.

3. The J" value was determined to be 34.5 $\pm$ 1 from the 529 nm excited
    fluorescence spectrum. The System XXII 0-0 excitation spectrum
    removes the $\pm$ 1 unit ambiguity and requires that J" = 34.5 (15).

Figure Caption

Figure 1. Partial Level Diagram for Systems XX and XXII Fluorescence.
The fluorescence spectra show that System XX and the 5287Å
excited system (* now known to be System XXII) share a common
lower level. The ΔT_0 values shown are band origin differences
whereas the $\Delta \nu$ values are separations between Q(33.5) lines.
Only $v'' = 0$ levels are shown.

-50-
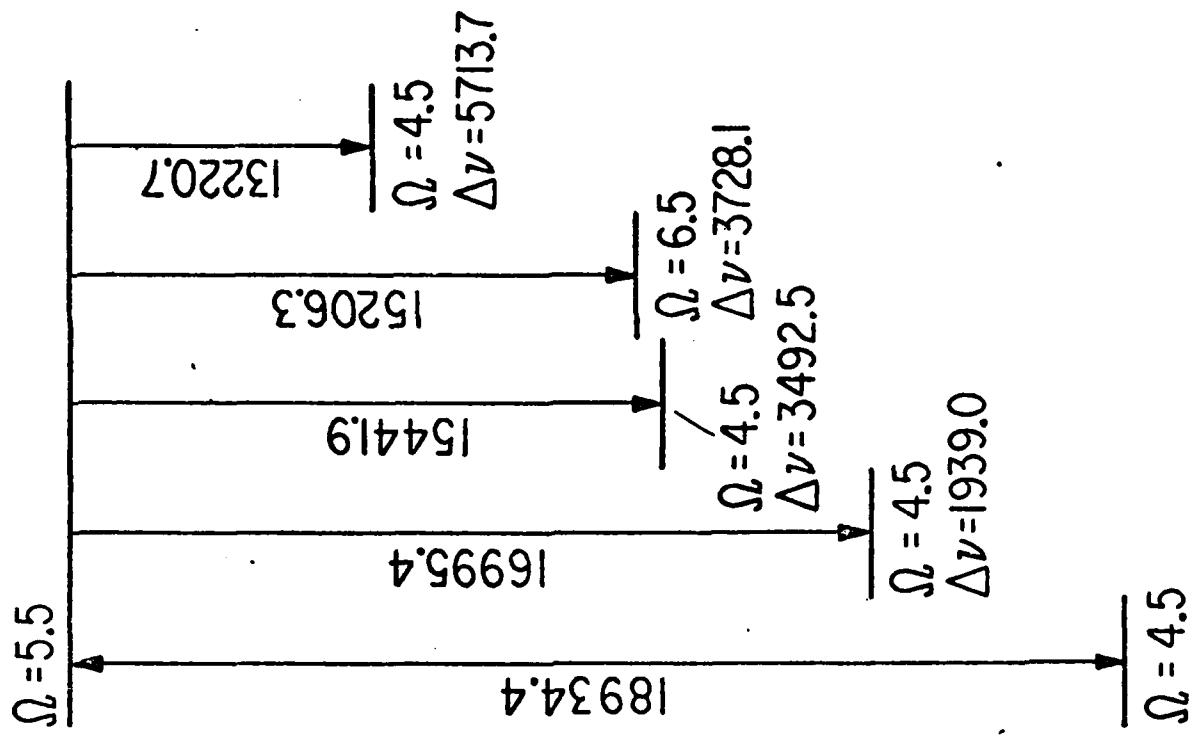
FIGURE 1

Table 1.   XX 0-0   Band Rotational Lines in cm^{-1}.[a]

J	R(J)	Q(J)	P(J)
4.5	17 846.068(3)[b]	-	-
5.5	17 846.710(-1)[b]	-	-
6.5	17 847.343(-1)[b]	-	17 837.360(-20)[b,c]
7.5	17 847.964(-1)[b]	-	17 836.560(-17)[b,c]
8.5	17 848.573(-1)[b]	-	17 835.750(-13)[b,c]
9.5	17 849.172(1)[b]	-	17 834.922(-15)[b,c]
10.5	17 849.756(0)[b]	-	-
11.5	17 850.329(0)[b]	-	-
12.5	17 850.889(0)[b]	-	-
13.5	17 851.434(-3)[b]	-	-
14.5	17 851.972(-1)[b]	-	-
15.5	17 852.496(0)[b]	17 840.758(2)	17 829.723(-4)
16.5	17 853.005(-2)[b]	17 840.559(3)	17 828.816(-1)
17.5	17 853.503(-2)[b]	17 840.346(2)	17 827.890(-3)
18.5	17 853.991(-1)	17 840.123(4)	17 826.959(2)
19.5	17 854.465(0)	17 839.886(4)	17 826.008(-1)
20.5	17 854.926(0)	17 839.635(2)	17 825.051(2)
21.5	17 855.376(2)	17 839.373(2)	17 824.075(-2)
22.5	-	17 839.094(-2)	-
23.5	17 856.236(3)	17 838.812(3)	17 822.089(-6)
24.5	17 856.644(0)	17 838.508(-2)	17 821.088(2)
25.5	17 857.043(2)	17 838.196(-2)	17 820.066(2)
26.5	17 857.425(-1)	17 837.872(-1)	-

Table 1. (continued)

J	R(J)	Q(J)	P(J)
27.5	17 857.795(-2)	17 837.534(-1)	-
28.5	17 858.149(-7)	17 837.184(-1)	17 816.918(-4)
29.5	17 858.500(-2)	17 836.820(-1)	-
30.5	17 858.834(0)	17 836.447(2)	17 814.757(-7)
31.5	17 859.155(1)	17 836.056(0)	-
32.5	17 859.459(-1)	17 835.654(0)	-
33.5	-	17 835.240(2)	-
34.5	-	17 834.812(0)	-

[a]Numbers in parentheses are (observed minus calculated) in units of $10^{-3} cm^{-1}$.

[b]Rotational line centers corrected for hyperfine structure.

[c]Blended line, not used in fit.

Table 2.   XX 0-0   Band Rotational and Hyperfine Constants in cm^{-1}.[a]

	$\Omega'' = 4.5$	$\Omega' = 5.5$
$\nu_{00} = T_0$	0.0	17 845.737(1)
B_0	0.361918(22)	0.355904(23)
$D_0 \times 10^7$	1.78(16)	2.60(17)
d_0[b]	0.2816(17)	0.1328(15)
d_J	$6.67(54) \times 10^{-5}$	
ν_{head}(calculated)	17 862.688 [R(53.5)]	
ν_{head}(observed)[c]	17 863.0	

---

[a]Uncertainties in parentheses represent one standard deviation

[b]$d'' = d_0 - d_J \, J(J+1)$

[c]Reference (1).

Table 3. Selected Hyperfine Lines of the XX $0-0$ Band in cm^{-1}.[a]

R(J)	F"	ν_{hfs}	$\Delta\nu_{observed}$
4.5	2	17 846.438	
			0.070(-3)
	3	846.368	
			0.096(1)
	4	846.272	
			0.130(-1)
	5	846.142	
			0.161(0)
	6	845.981	
			0.196(0)
	7	845.785	
5.5	3	17 846.995	
			0.062(-2)
	4	846.933	
			0.082(2)
	5	846.851	
			0.104(-1)
	6	846.747	
			0.122(0)
	7	846.625	
			0.143(-1)
	8	846.482	
6.5	4	17 847.575	
			0.060(-1)
	5	847.515	
			0.066(-6)[b]
	6	847.449	
			0.092(7)[b]
	7	847.357	
			0.097(1)
	8	847.260	
			0.109(1)
	9	847.151	

Table 3. (Continued)

R(J)	F"	ν_{hfs}	$\Delta\nu_{observed}$
7.5	5	17 848.158	
	6	848.106	0.052(1)
	7	848.045	0.061(2)
	8	847.972	0.073(-1)
	9	847.890	0.082(-1)
	10	847.800	0.090(-1)
8.5	6	17 848.739	
	7	848.690	0.049(-1)
	8	848.635	0.055(0)
	9	848.573	0.062(0)
	10	848.506	0.067(2)
	11	848.432	0.074(1)
9.5	7	17 849.319	
	8	849.274	0.045(-1)
	9	849.224	0.050(-1)
	10	849.170	0.054(1)
	11	849.109	0.061(-1)
	12	849.041	0.068(4)

Table 3. (Continued)

R(J)	F"	ν_{hfs}	$\Delta\nu_{observed}$
10.5	8	17 849.884	
	9	849.844	0.040(0)
	10	849.800	0.044(0)
	11	849.752	0.048(0)
	12	849.701	0.051(1)
	13	849.646	0.055(1)
11.5	9	17 850.443	
	10	850.406	0.037(-1)
	11	850.367	0.039(1)
	12	850.324	0.043(0)
	13	850.278	0.046(0)
	14	850.228	0.050(-1)
12.5	10	17 850.991	
	11	850.958	0.033(0)
	12	850.921	0.037(-1)
	13	850.882	0.039(0)
	14	850.839	0.043(-1)
	15	850.794	0.045(-1)

Table 3. (Continued)

R(J)	F"	ν_{hfs}	$\Delta\nu_{observed}$
13.5	11	17 851.528	
			0.030(1)
	12	851.498	
			0.032(1)
	13	851.463	
			0.035(0)
	14	851.427	
			0.036(2)
	15	851.391	
			0.039(1)
	16	851.352	
14.5	12	17 852.054	
			0.025(-3)[b]
	13	852.029	
			0.032(2)[b]
	14	851.997	
			0.032(0)[b]
	15	851.965	
			0.034(0)[b]
	16	851.931	
			0.035(-1)[b]
	17	851.896	

P(J)	F"	ν_{hfs}	$\Delta\nu_{observed}$
6.5	4	17 837.510	
			0.050(4)
	5	837.460	
			0.049(-2)
	6	837.411	
			0.055(0)
	7	837.356	
			0.056(-2)
	8	837.300	
			0.060(-2)
	9	837.240	

Table 3. Continued

P(J)	F"	ν_{hfs}	$\Delta\nu_{observed}$
7.5	5	17 836.688	
	6	836.648	0.040(-2)
	7	836.603	0.045(-1)
	8	836.554	0.049(-1)
	9	836.502	0.052(0)
	10	836.449	0.053(-3)
8.5	6	17 835.871	
	7	835.835	0.036(-2)
	8	835.797	0.038(-4)
	9	835.749	0.048(4)
	10	835.702	0.047(-1)
	11	835.654	0.048(-3)

[a]Numbers in parentheses represent observed - calculated in 10^{-3} cm^{-1}.

[b]These values were not included in the fit because of blending.

Table 4. $\Delta F = 0$ Hyperfine Transitions of XX 0-0.

F'	F"	ν (cm^{-1})	$\Delta\nu$ (cm^{-1})[a]	Intensity Ratio Observed	Calculated
R(4.5)					
3	3	-	0.081[b]	-	7.8
4	3	17 846.368			
4	4	17 846.171	0.101(0)	-	6.2
5	4	17 846.272			
5	5	17 846.022	0.120(-2)	3.5	6.8
6	5	17 846.142			
6	6	17 845.838	0.143(0)	3.2	9.2
7	6	17 845.981			
7	7	17 845.623	0.162(-2)	4.2	17.5
8	7	17 845.785			
R(7.5)					
10	10	17 847.694	0.106(8)	-	-
11	10	17 847.800			
R(8.5)					
11	11	17 848.349	0.083(-3)	-	-
12	11	17 848.432			
R(9.5)					
12	12	17 848.968	0.073(-4)	-	-
13	12	17 849.041			
R(10.5)					
13	13	17 849.579	0.067(-3)	-	-
14	13	17 849.646			
R(11.5)					
14	14	17 850.166	0.062(-2)	-	-
15	14	17 850.228			
R(12.5)					
15	15	17 850.738	0.056(-3)	-	-
16	15	17 850.794			
R(13.5)					
16	16	17 851.296	0.056(-2)	-	-
17	16	17 851.352			

[a]Quantities in parentheses are observed minus calculated in 10^{-3} cm^{-1}.
[b]Calculated splitting. The F' ← F" 3,3 and 5,4 hyperfine lines are blended.

Table 5. Summary of Constants Derived from XX 0-0 Band Fluorescence Spectra[a]

Ω	ν_{00}	B_0	α_e	$D_0 \times 10^7$
5.5	17 845.737(1)	0.355904(23)	-	2.60(17)
4.5	3 500.3(3)[e]	0.3556(3)	-	1.78
4.5	1 936.7(2)[c,d]	0.3637(2)	0.0018(4)	1.78
4.5	0.0[b]	0.361918(22)	0.0014(3)	1.78(16)

[a]Uncertainties in parentheses are one standard deviation.

[b]$\Delta G_{1/2}$ = 831.8(4)

[c]$\Delta G_{1/2}$ = 833.0(4)

[d]Ω' = 5.5 - Ω'' = 4.5 ν_{head}(calculated) = 15 921.9 (R branch)

[e]Ω' = 5.5 - Ω'' = 4.5. The head occurs at very high J in P branch and the band should appear to be headless.

The Electronic Spectrum of PrO. Energy Linkages, Rotational Analysis, and Hyperfine Structure for Systems XVII and XXI

Michael Dulick and Robert W. Field
Spectroscopy Laboratory and Department of Chemistry
Massachusetts Institute of Technology
Cambridge, Massachusetts 02139

and

J. Cl. Beaufils and J. Schamps
Laboratoire de Spectroscopie des Molecules Diatomiques
Universite des Sciences et Techniques de Lille
U.E.R. de Physique Fondamentale, Bat. P.5
59655 Villeneuve d'Ascq Cedex, FRANCE

13 Pages

4 Tables (14 pages)

1 Figure

Proposed Running Head:

PrO Systems XVII and XXI

Send proofs and all correspondence to:

Professor Robert W. Field
Department of Chemistry, 6-223
Massachusetts Institute of Technology
Cambridge, Massachusetts 02139

List of Symbols

Ω Cap. Greek omega

β l.c. Greek beta

λ l.c. Greek lambda

$\neq$ not equal to

$<$ less than

$>$ greater than

Δ Cap. Greek delta

Λ Cap. Greek lambda

Σ Cap. Greek sigma

Pr III   Cap. pea, small R, space, half-size Roman numeral 3; designates doubly ionized praseodymium

σ l.c. Greek sigma

Abstract

Doppler-limited laser excitation spectra for four bands of PrO have been recorded: System XVII 0-0, System XXI 0-0 and 0-1, and the 0-0 intercombination between the upper and lower states, respectively, of Systems XVII and XXI. First lines in R and P branches prove that Systems XVII and XXI are, respectively, $\Omega' = 4.5 - \Omega'' = 3.5$ and $\Omega' = \Omega'' = 4.5$. Hyperfine components are well-resolved for all four excitation bands. Rotational and hyperfine constants are determined by least squares fits of data from all four bands together. In addition, fluorescence spectra, recorded from various J', $v' = 0$ levels of the upper states of Systems XVII and XXI, reveal five new low-lying states. Principal constants (in cm^{-1}) for nine Ω-states follow (1σ uncertainty in parentheses):

State	T_v	B_v	d(hfs)
$\Omega' = 4.5$ (System XXI)	18 882.388 (2)	0.353001 (18)	0.12403 (71)
$\Omega' = 4.5$ (System XVII)	16 594.075 (1)	0.353736 (20)	0.12977 (67)
$\Omega'' = 3.5$	3 887.15 (16)	0.35751 (28)	-
$\Omega'' = 3.5$	2 931.66 (15)	0.35712 (21)	-
$\Omega'' = 4.5$	2 155.16 (30)	0.36264 (67)	-
$\Omega'' = 3.5$	2 099.16 (31)	0.35079 (71)	-
$\Omega'' = 3.5$	2 064.34 (13)	0.35654 (20)	-
$\Omega'' = 4.5$ (System XXI)	217.383 (1)	0.362134 (20)	0.27744 (66)
$\Omega'' = 3.5$ (System XVII)	0.0	0.360948 (16)	-0.00809 (85)

I. Introduction

The 22 electronic transition reported by Shenyavskaya et al. (1) indicate
that the electronic structure of the PrO molecule is extremely complex and
that construction of a reasonably complete energy level diagram for E < 25 000 cm^{-1}
will be a formidable task. The preceeding paper (2) suggests that there are
many more than 22 electronic systems involving the lowest electronic states of
PrO. In that paper, it was possible, for the first time, to arrange several electronic
states into a partial energy level diagram. In this paper we present another
partial level diagram, based on laser induced fluorescence spectra resulting
from excitation of specific transitions in the System XVII 0-0 and XXI 0-0 bands.
The two groups of states discussed here and in the preceeding paper (2) cannot,
at present, be unambiguously linked to each other.

An indication of the expected complexity of the electronic structure of
PrO is obtained from the following considerations. Among the lowest energy
configurations, one expects $Pr^{+2}O^{-2}$ with three electrons in Pr^{+2}-centered,
$6s4f^2$ nonbonding orbitals. From this configuration alone one expects 91 case 'c'
molecular states as follows:

Ω	J_a = 6.5	5.5	4.5	3.5	2.5	1.5	0.5	Total
6.5	2							2
5.5	2	3						5
4.5	2	3	4					9
3.5	2	3	4	4				13
2.5	2	3	4	4	4			17
1.5	2	3	4	4	4	4		21
0.5	2	3	4	4	4	4	3	24

Number of Ω-States

each of which is doubly degenerate. Hund's rules suggest a lowest lying Pr $\underline{III}$ $^4H_{3.5}$ state which will be split by the O^{-2} ^1S ligand into Ω = 3.5, 2.5, 1.5, and 0.5 molecular states, in order of expected increasing energy. The fact that we report here several low lying Ω = 3.5 states is interesting, if not significant.

In addition to states with $6s4f^2$ parentage, one might expect $6s^24f$, $6s5d4f$, and $4f^3$ states. These should be recognizable from differences in hyperfine coupling constants. It may be significant that the magnetic hyperfine structure of the lower state of System XVII is significantly smaller than that for the upper state of System XVII and both states of Systems XX and XXI.

This paper presents the analysis of rotational and hyperfine structure for the System XVII 0-0 (602 nm), XXI 0-0 (535 nm), and 0-1 (560 nm) bands and the 0-0 band (610 nm) of a newly identified intercombination system involving the upper state of System XVII and the lower state of System (XXI). For conciseness, this system will hereafter be referred to as XVII-XXI. In addition, spectra of fluorescence excited from v' = 0 levels of Systems XVII and XXI have led to identification of five new v' = 0 levels (four Ω=3.5, one Ω=4.5, zero Ω=5.5) approximate rotational constants for these levels, and an energy linkage of Systems XVII and XXI through XVII-XXI and XXI-XVII intercombination bands (610 and 529 nm).

II. Experiment

Experimental conditions were identical to those reported in the preceeding paper (2) with the exception that Rhodamine 6G and 110 dyes were used, respectively, to record the spectra (excitation and fluorescence) for Systems XVII and XXI.

III. Description of Excitation and Fluorescence Spectra

The System XVII 0-0 band (Table 1A) is red degraded, has a bandhead at 601.89 nm ($\underline{1}$),
and includes three branches with intensities $I_Q \gg I_R > I_P$. The first lines
in the R and P branches are found to be R(3.5) and P(5.5). The resolved
fluorescence method for identifying first lines employed here is free of
interference by overlapping lines, in constrast to classical spectroscopy.
The present analysis confirms that System XVII involves an $\Omega' = 4.5 - \Omega'' = 3.5$
transition ($\underline{3}$).

The System XXI 0-0 and 0-1 bands (Table 1B) are red degraded, with heads at 535.20
and 560.06 nm ($\underline{1}$), and consist of three branches with intensities $I_P = I_R \gg I_Q$.
The weak Q branch is found only at low J values. The first lines in the R
and P branches are found to be R(4.5) and P(5.5), which implies that System XXI
involves an $\Omega' = 4.5 - \Omega'' = 4.5$ $\Delta\Omega = 0$ transition.

As was the case for System XX ($\underline{2}$), hyperfine splittings are resolvable,
under Doppler-limited conditions, for low-J lines of Systems XVII and XXI (Table 2A and B).
There are always six strong components, corresponding to the $\Delta F = \Delta J$ selection
rule. Additional weak $\Delta F = 0$, $\Delta J = +1$ components are observed for the first few R lines
in both systems. The intensity pattern of the hyperfine components of the
P, Q, and R lines of both systems is consistent with case 'a_β' (or 'c_β')
coupling.

The hyperfine components of each P, Q, and R line of System XVII 0-0 are
shaded to shorter wavelengths. In other words, $F''_{min} = J'' - 5/2$ is always at
longer λ than $F''_{max} = J'' + 5/2$. When the hyperfine splittings of P(J'') with
R(J'') and P(J'' + 1) with R(J'' - 1) line pairs are compared, by far the larger
hyperfine splitting is found to occur in the upper electronic state ($\Omega' = 4.5$).
The hyperfine shading of P and R lines for System XXI 0-0 and 0-1 bands is

in the opposite sense to that found in System XVII 0-0. Comparison of P, R
line pairs with common J" and J' values leads to the conclusion that the
larger hyperfine splitting occurs in the lower state (Ω" = 4.5). The upper
state (Ω' = 4.5) hfs is approximately 50% as large as that in the lower state.

The rotational structure of the System XVII 0-0 band is perturbed in the
upper state (Table 1D). Level shifts and extra lines become noticable by J' = 21.5
One set of extra lines appears to cross the main lines from above at J' $\overset{\sim}{\sim}$ 23.0.
However, for only the two J' values on either side of this crossing an additional
set of (weak) extra lines is present, corresponding to an additional state
crossing both the main and stronger perturber from above. The original series
of extra lines disappears by J' = 25.5, but a residual shift of R, Q, and P
lines persists to higher J' values. Beyond J' = 29.5, all lines split into
two components of about equal intensity with splitting proportional to J (J+1).
Near the J = 23 crossing, both sets of extra lines are far broader than their
predicted Doppler widths (as well as broader than the unperturbed main lines),
thus suggesting that both perturbing states have unusually large hyperfine
structure. A detailed discussion of these perturbations must await Ω assignments
and low-J resolved hfs for the perturbers.

When individual rotational lines of the System XVII 0-0 band near 602 nm
are laser excited, five 0-0 bands are observed (in addition to XVII 0-0) in
the resultant fluorescence spectrum. These bands are located at approximately
610, 688, 730, 732, and 787 nm. A similar spectrum excited via XXI 0-0 near
535 nm contains five 0-0 bands (in addition XXI 0-0) at 530, 595, 596, 598, and
667 nm and three 0-1 bands, 625, 627, and 667 nm.

In Section IVC we show that the 530 and 610 nm fluorescence bands are
XXI-XVII Ω' = 4.5- Ω" = 3.5 and XVII-XXI Ω' = 4.5-Ω" = 4.5 intercombination bands,

respectively. High resolution, Dopper-limited excitation spectra were recorded
for the 610 nm band, which was found to consist of strong P and R lines and
weaker Q lines observable through J = 30.5. The relative branch intensities
and observed first lines, R(4.5) and P(5.5), demonstrate that this band is
$\Omega' = \Omega'' = 4.5$, in agreement with the XVII-XXI assignment. Large hyperfine
splittings in R and P lines are resolvable through R(19.5) and P(19.5). The
hyperfine components are shaded to longer wavelength $[\lambda(F_{min}) < \lambda(F_{max})]$.
Comparison of hyperfine splitings in P and R lines indicates, as expected,
larger hfs in the lower state. Finally, rotational perturbations in the upper
state exactly match those in the System XVII 0-0 band.

IV. Results

A. Rotational Analysis

The rotational lines of the XVII 0-0, XXI 0-0 and 0-1, and XVII-XXI 0-0
bands are listed in Table 1. For those low-J lines with resolvable hfs,
centers-of-gravity are computed from measured hyperfine components.

B. Hyperfine Analysis

Measured hyperfine components are listed in Table 2, along with observed
and calculated splittings between components. The splittings and intensities
are well represented by case 'a_β' coupling.

The magnetic hyperfine constants for the upper and lower v' = v" = 0 levels
of Systems XVII and XXI as well as v" = 1 of System XXI were obtained from a
simultaneous, nonlinear, least squares fit to all resolved hfs from the four
bands cited in Section IVA. The fitting procedure employed the Davidon-Fletcher-
Powell (4) algorithm and the hyperfine energy level expressions from the
preceeding paper (2). $\Delta J \neq 0$ hyperfine matrix elements necessitated iterative
fitting; the convergence criterion for the hfs parameters was 1 in 10^4.

This simultaneous fit of hfs from four bands involving three electronic states has significantly reduced correlation between upper and lower state hyperfine constants. One important result is that it has been possible to obtain a statistically significant value for the very small hyperfine constant for the lower state of System XVII. Quadrupole interaction terms were found to be statistically indistinguishable from zero (ΔeQq < 20 MHz).

The rotational and hyperfine constants for the upper and lower levels of the four bands recorded at high resolution are listed in Table 3.

C. Analysis of Fluorescence Spectra

The dye laser was tuned to excite known P(J) or Q(J) lines of the System XVII and XXI 0-0 bands. Thus term energies and J' values are known without ambiguity for all lines appearing in the resultant fluorescence spectra. Ω" assignments for the lower states observed in fluorescence were based on low-J P vs. R relative intensities and the presence or absence of Q lines. At low-J, all intensity anomalies, which arise from parallel vs. perpendicular transition interference effects, vanish because the heterogeneous perturbation matrix element responsible vanishes as J $\longrightarrow$ 0 (5).

The energy levels of Systems XVII and XXI were linked through these fluorescence spectra. A band, containing strong P and R lines and very weak Q lines ($\Delta\Omega$ = 0), was found approximately 217 cm^{-1} to the red of the System XVII 0-0 band. Another band, 217 cm^{-1} to the blue of the System XXI 0-0 band, was found which exhibited I_Q >> I_R > I_P ($\Delta\Omega$ = +1). These two bands were assigned as XVII-XXI and XXI-XVII intercombination bands. These assignments are supported by the following: first, all fluorescence bands observed upon excitation in System XVII correspond to levels observed in fluorescence excited via System XXI (only the 598 nm band from System XXI has no System XVII counterpart); second,

the rotational and hyperfine constants derived from the 610 nm XVII-XXI
intercombination band (Tables 1C and 2C) exactly match those for the upper and lower states.
respectively, of Systems XVII and XXI; third, the upper state perturbations
in the XVII and XVII-XXI 0-0 bands match perfectly.

Table 4 presents T_0 (relative to zero for the lower state of System XVII)
and B_0 values derived from least squares fits to all fluorescence lines
resulting from excitations in System XVII and XXI 0-0 bands. The measurement
accuracy for the lines in the fluorescence spectra, ± 0.3 cm^{-1}, is insufficient
to allow determination of centrifugal distortion constants.

Figure 1 is a level diagram summarizing the energies and Ω-values for all
states of PrO observed in the excitation and fluorescence spectra discussed in
this paper. A similar level diagram is presented in the preceeding paper (2),
but no linkage between the states shown on these two diagrams can, at present,
be demonstrated.

V. Discussion

Although the rotational and vibrational constants of PrO for all states
discussed in this and the previous paper (2) vary by at most 1%, the hyperfine
constants exhibit a huge range of variation. In particular, the lower state
of System XVII ($\Omega'' = 3.5$) possesses an extremely small magnetic hfs, suggesting
that it is derived from a configuration with no 6s Pr electrons. The
larger hfs of the upper and lower systems of Systems XX and XXI and the upper
state of System XVII could be consistent with single occupancy of a Pr 6s
orbital. Since the electron spin of these states is unknown (and probably
ill-defined because of strong spin-orbit mixing), it is not possible to report
the usual Fermi-contact hyperfine constant for each state. However, it should

be pointed out that if the lower states of Systems XX and XXI are doublets, then their Fermi-contact terms would be 0.554 cm^{-1}, in reasonable agreement with the corresponding term for $4f^2 6s$ levels of the free Pr III ion (6). (The precision of hfs constants from Pr III spectra are considerably poorer than for the molecular hfs reported here.)

It is premature to speculate further about the configurational parentages of the observed states of the PrO molecule. It is clear from the small range of variation for rotational and vibrational constants that these electronic states differ only by which three of the numerous (fourteen 4f, ten 5d, two 6s) nonbonding, Pr^{+2}-centered spin-orbitals are occupied. The often-ignored Hund's case 'c' quantum number, J_a (total angular momentum of the Pr III ion), is likely to be useful in understanding perturbations and transition intensity patterns. For example: of the multitude of predicted $\Omega = 3.5$ and 4.5 states, those belonging to the same J_a will appear together in the fluorescence spectrum from a single upper state; of transitions sharing a common state, those with $\Delta\Omega = \Delta J_a$ will be strongest (if $J_a \approx \ell$) and those with $|\Delta J_a| > 1$ should be very weak. It is likely that the upper states of Systems XVII and XXI share a common J_a (probably 4.5) which is different from the J_a value (probably 5.5) of the System XX (and possibly XXII) upper state.

It is hoped that continuing investigations of Systems XXII, XVI, and XV (7),combined with results from Shenyavskaya et al. (8),will permit more definitive J_a and configurational assignments as well as construction of a complete energy level diagram for E < 25000 cm^{-1}

Acknowledgments

References

1. E. A. Shenyavskaya, I. V. Egorova, and V. N. Lupanov , J. Mol. Spectrosc. 47, 355-362 (1973).

2. M. Dulick, J. Cl. Beaufils, and R.W. Field, J. Mol. Spectrosc. (preceeding paper).

3. M. Dulick, R.W. Field, and J.Cl. Beaufils, J. Mol. Spectrosc. 78, 333-334 (1979).

4. D.M. Himmelblau, Applied Non-Linear Programming, p. 111-121, McGraw-Hill, N.Y. 1972.

5. R.A. Gottscho, J.B. Koffend, J.R. Lombardi, and R.W. Field, J. Chem. Phys. 68, 4110-4122 (1978).

6. J. Sugar, J. Opt. Soc. Am. 53, 831-839 (1963).

7. M. Dulick, unpublished.

8. E.A. Shenyavskaya and L.A. Kaledin, Talk E2, Molecular Spectroscopy Conference, 1979, Tours, France.

Figure Captions

Figure 1. Partial Level Diagram for Systems XVII and XXI. The dotted
(solid) lines indicate the System XVII (XXI) 0-0 excitation
band and all resultant 0-0 fluorescence bands. Note that all
but one lower $v'' = 0$ level appear in fluorescence spectra
excited via Systems XVII and XXI.
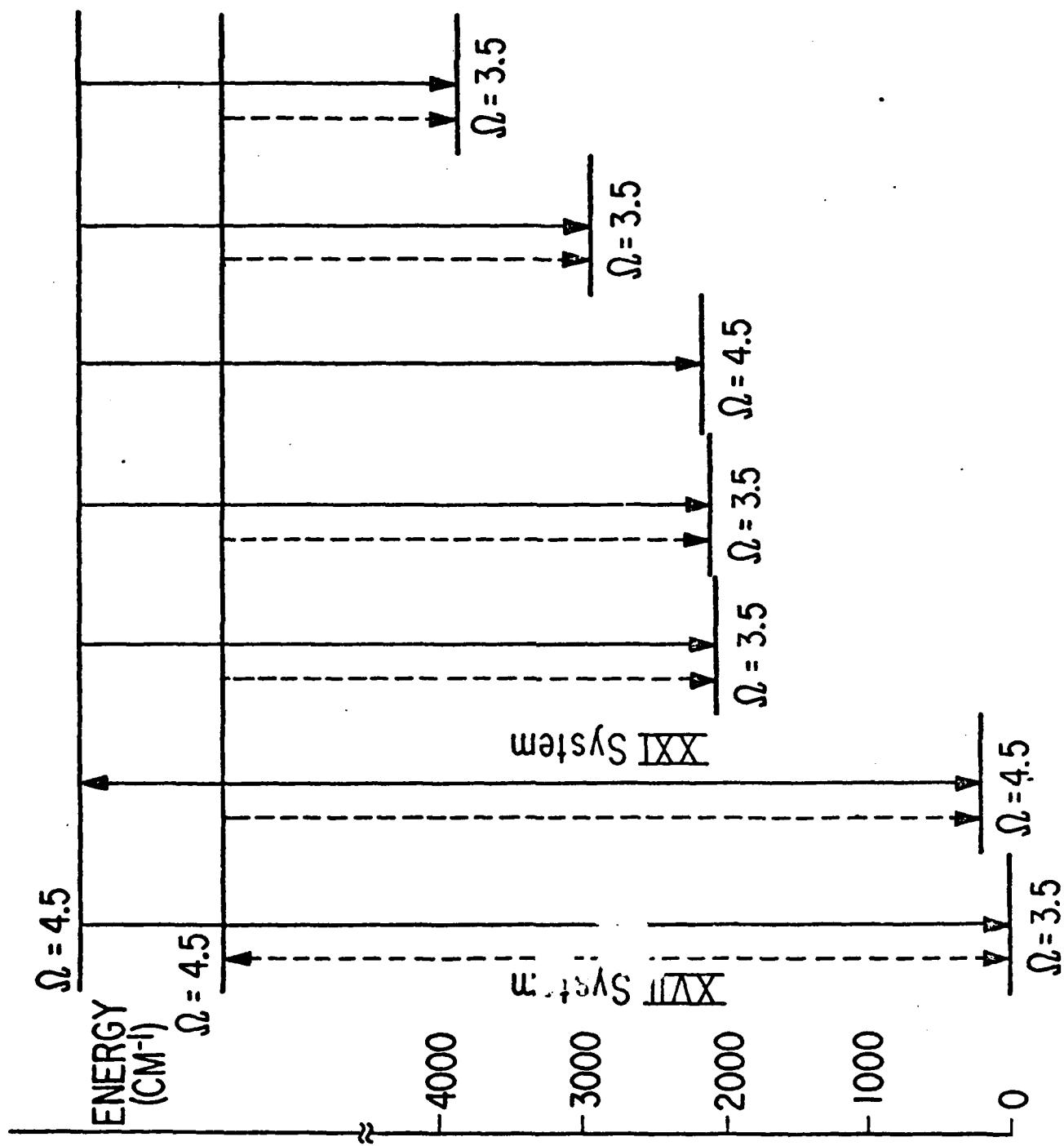
FIGURE 1

Table 1A· System XVII (Ω' = 4.5 - Ω'' = 3.5) Rotational Lines (in cm^{-1})[a,b]

0-0 Band

J	R(J)		Q(J)		P(J)	
3.5	16 594.406	(2)	-	-	-	-
4.5	595.047	(1)	-	-	-	-
5.5	595.675	(1)	-	-	16 587.191	(6)
6.5	596.287	(0)	-	-	586.379	(-5)
7.5	596.884	(-2)	-	-	585.562	(-6)
8.5	597.471	(1)	-	-	584.732	(-6)
9.5	598.038	(-1)	-	-	583.896	(2)
10.5	598.592	(-2)	-	-	583.041	(7)
11.5	599.134	(0)	-	-	582.163	(2)
12.5	599.661	(2)	-	-	581.276	(3)
13.5	600.170	(1)	16 589.910	(-6)	580.375	(5)
14.5	600.664	(0)	589.699	(-6)	579.456	(3)
15.5	601.144	(0)	589.474	(-5)	578.525	(4)
16.5	601.610	(1)	589.230	(-8)	577.573	(-1)
17.5	-	-	588.480	(-3)	576.614	(2)
18.5	602.490	(-3)	588.712	(-10)	575.642	(6)
19.5	602.905	(-8)	588.426	(0)	574.650	(6)
20.5	-	-	588.123	(-2)	573.645	(7)

[a]Numbers in parentheses are observed minus calculated, in 10^{-3} cm^{-1}.

[b]Degeneracy weighted centers of gravity calculated from resolved hyperfine components

Table 1B. System XXI (Ω' = 4.5 - Ω'' = 4.5) Rotational Lines (in cm⁻¹)[a,b]

J	0-0 Band			0-1 Band [c]	
	R(J)	Q(J)	P(J)	R(J)	P(J)
4.5	18 668.845 (-3)	-	-	17 837.200 (-1)	-
5.5	669.455 (2)	-	18 660.978 (-4)	17 837.824 (2)	17 829.350 (-1)
6.5	670.038 (-2)	-	660.157 (0)	838.423 (-5)	17 828.548 (3)
7.5	670.609 (0)	-	659.314 (0)	839.016 (-2)	827.722 (-1)
8.5	671.15: (-3)	-	658.454 (1)	839.595 (2)	826.887 (1)
9.5	671.688 (-4)	-	657.569 (-5)	840.153 (1)	826.037 (3)
10.5	672.210 (4)	-	656.677 (0)	840.696 (0)	825.167 (0)
11.5	672.707 (5)	-	655.764 (2)	841.226 (2)	824.283 (-1)
12.5	673.183 (4)	-	654.830 (2)	841.740 (3)	823.386 (0)
13.5	673.640 (1)	-	653.876 (-1)	842.235 (1)	822.472 (-1)
14.5	674.079 (-1)	18 663.148 (7)	652.907 (0)	842.716 (-1)	821.538 (-6)
15.5	674.506 (4)	662.862 (4)	-	-	820.596 (-5)
16.5	674.908 (1)	662.559 (1)	650.912 (-2)	-	-
17.5	675.292 (-1)	-	649.891 (1)	844.493 (2)	818.660 (-8)
18.5	675.658 (-3)	661.902 (-1)	648.851 (2)	844.893 (-3)	817.672 (-7)
19.5	676.010 (-1)	661.547 (-1)	647.789 (-1)	845.285 (-1)	816.673 (-2)
20.5	676.338 (-5)	661.172 (-3)	646.714 (2)	845.660 (-1)	815.652 (-3)
21.5	676.652 (-5)	660.784 (-1)	645.615 (-2)	846.025 (5)	814.618 (-3)
22.5	676.960 (8)	660.370 (-6)	644.502 (-2)	846.368 (4)	-
23.5	677.232 (2)	659.964 (15)	643.375 (2)	846.696 (3)	-
24.5	677.498 (9)	659.509 (4)	-	847.007 (0)	-
25.5	677.730 (0)	659.044 (1)	-	847.307 (2)	-
26.5	677.952 (-1)	658.559 (-3)	-	847.586 (-2)	-
27.5	678.155 (-4)	658.058 (-6)	-	847.850 (-7)	-
28.5	678.339 (-7)	-	-	-	-
29.5	678.519 (4)	-	-	-	-
30.5	678.673 (6)	-	-	-	-
31.5	678.799 (-1)	-	-	-	-
32.5	678.913 (-3)	-	-	-	-
33.5	-	-	-	-	-
34.5	679.094 (1)	-	-	-	-

[a] Numbers in parentheses are observed minus calculated, in 10⁻³ cm⁻¹.

[b] Degeneracy weighted centers of gravity calculated from resolved hyperfine components.

[c] Q branch is too weak to record.

Table 1C. Intercombination: Upper State System XVII - Lower State System XXI
($\Omega' = 4.5 - \Omega'' = 4.5$) Rotational Lines (in cm^{-1})[a,b]

0-0 Band

J	R(J)		R(P)	
4.5	16 380.550	(4)	-	-
5.5	381.164	(4)	16 372.671	(-1)
6.5	381.760	(2)	371.853	(-2)
7.5	382.340	(1)	371.019	(-3)
8.5	382.904	(1)	-	-
9.5	383.452	(2)	369.300	(-4)
10.5	383.980	(0)	368.418	(-3)
11.5	384.491	(-1)	367.519	(-1)
12.5	384.988	(0)	366.600	(-2)
13.5	385.465	(-1)	365.665	(-2)
14.5	385.926	(-1)	364.714	(-2)
15.5	386.370	(-1)	363.746	(-1)
16.5	386.798	(1)	362.761	(-1)
17.5	387.207	(2)	361.759	(0)
18.5	387.598	(2)	360.742	(3)
19.5	387.970	(0)	359.705	(3)

[a]Numbers in parentheses are observed minus calculated, in 10^{-3} cm^{-1}.

[b]Degeneracy weighted centers of gravity calculated from resolved hyperfine components.

Table 1D. Main and Extra Lines Near the First Perturbation in the Upper State of the XVII 0-0 Band (in cm^{-1})

J	R(J)			Q(J)			P(J)		
	Main	Extra	Weak-Extra	Main	Extra	Weak-Extra	Main	Extra	Weak-Extra
20.5	16 603.286	16 603.431							
21.5	603.725	603.641		16 587.770	16 587.913				
22.5	604.183	604.065		587.405	587.488	16 587.653	16 571.560	16 570.700	
23.5	604.511	604.368		587.238	587.121		570.471	570.553	16 570.715
24.5							569.573	569.456	569.327
25.5							568.463	568.323	

Table 2A. System XVII 0-0 Band Hyperfine Lines (in cm^{-1})

J'	F'	R(F', J'')	-Δν[a]		P(F', J'')	-Δν[a]	
3.5	1	16 594.069	0.073	(1)[b]			
	2	594.142	0.097	(0)			
	3	594.239	0.121	(-1)			
	4	594.360	0.146	(-1)			
	5	594.506	0.172	(-1)			
	6	594.678					
4.5	2	594.775	0.067	(1)			
	3	594.842	0.083	(0)			
	4	594.925	0.100	(0)			
	5	595.025	0.115	(-1)			
	6	595.140	0.133	(0)			
	7	595.273					
5.5	3	595.449	0.060	(0)	16 586.861	0.070	(-1)[b]
	4	595.509	0.072	(0)	586.931	0.096	(1)
	5	595.581	0.084	(0)	587.027	0.119	(0)
	6	595.665	0.096	(0)	587.146	0.145	(1)
	7	595.761	0.107	(-1)	587.291	0.169	(1)
	8	595.868			587.460		
6.5	4	596.093	0.056	(2)	586.109	0.068	(2)
	5	596.149	0.063	(0)	586.177	0.089	(2)
	6	596.212	0.072	(0)	586.261	0.096	(2)
	7	596.284	0.081	(0)	586.357	0.116	(2)
	8	596.365	0.090	(0)	586.473	0.130	(0)
	9	596.455			586.603		
7.5	5	596.716	0.050	(1)	585.340	0.060	(0)
	6	596.766	0.057	(1)	585.400	0.070	(-1)
	7	596.823	0.063	(0)	585.470	0.083	(0)
	8	596.886	0.070	(0)	585.553	0.094	(0)
	9	596.956	0.077	(1)	585.647	0.105	(-1)
	10	597.033			585.752		
8.5	6	597.323	0.045	(0)	584.543	0.053	(-1)
	7	597.368	0.050	(0)	584.596	0.063	(0)
	8	597.418	0.057	(1)	584.659	0.071	(0)
	9	597.475	0.060	(-1)	584.730	0.078	(-2)
	10	597.535	0.067	(1)	584.808	0.089	(1)
	11	597.602			584.897		
9.5	7	597.908	0.041	(0)	583.732	0.049	(0)
	8	597.949	0.045	(0)	583.781	0.055	(-1)
	9	597.994	0.050	(1)	583.836	0.063	(1)
	10	598.044	0.054	(0)	583.899	0.068	(-1)
	11	598.098	0.058	(0)	583.967	0.075	(0)
	12	598.156			584.042		

J"	F"	R(F", J")	-Δν[a]		P(F", J")	-Δν[a]	
10.5	8	16 598.476			16 582.898		
	9	598.512	0.036	(-1)	582.941	0.043	(-1)
	10	598.554	0.042	(1)	582.991	0.050	(0)
	11	598.598	0.044	(0)	583.044	0.053	(-2)
	12	598.646	0.048	(0)	583.105	0.061	(1)
	13	598.698	0.052	(1)	583.170	0.065	(0)
11.5	9	599.031			582.035		
	10	599.064	0.033	(-1)	582.075	0.040	(0)
	11	599.064	0.037	(0)	582.120	0.045	(0)
	12	599.101	0.041	(1)	582.168	0.048	(-1)
	13	599.184	0.042	(-1)	582.221	0.053	(0)
	14	599.230	0.046	(0)	582.279	0.058	(1)
12.5	10	599.566			581.162		
	11	599.598	0.032	(1)	581.198	0.036	(-1)
	12	599.631	0.033	(0)	581.238	0.040	(0)
	13	599.667	0.036	(0)	581.282	0.044	(0)
	14	599.706	0.039	(1)	581.328	0.046	(-1)
	15	599.747	0.041	(0)	581.379	0.051	(0)
13.5	11	600.086			580.273		
	12	600.114	0.028	(0)	580.306	0.033	(-1)
	13	600.145	0.031	(1)	580.342	0.036	(0)
	14	600.178	0.033	(1)	580.381	0.039	(0)
	15	600.213	0.035	(1)	580.424	0.043	(1)
	16	600.250	0.037	(1)	580.468	0.044	(-1)
14.5	12	600.588			579.366		
	13	600.614	0.026	(0)	579.395	0.029	(-2)
	14	600.642	0.028	(0)	579.428	0.033	(0)
	15	600.671	0.029	(0)	579.463	0.035	(-1)
	16	600.703	0.032	(1)	579.501	0.038	(0)
	17	600.736	0.033	(0)	579.541	0.040	(0)
15.5	13	601.076			578.444		
	14	601.099	0.023	(0)	578.472	0.028	(0)
	15	601.123	0.024	(-1)	578.501	0.029	(-1)
	16	601.150	0.027	(0)	578.529	0.028	(-4)
	17	601.179	0.029	(1)	578.566	0.037	(3)
	18	601.209	0.030	(0)	578.603	0.037	(1)
16.5	14	601.550					
	15	601.569	0.019	(-2)			
	16	601.591	0.022	(-1)			
	17	601.616	0.025	(1)			
	18	601.641	0.025	(0)			
	19	601.669	0.028	(1)			

[a]For each hyperfine multiplet, the 5 tabulated differences between adjacent components were input to the hyperfine fit. Note that the hyperfine pattern in this band is degraded in the opposite sense to that for the other bands.

[b]Calculated minus observed, in 10^{-3} cm^{-1}.

Table 2B. **System XXI** - Hyperfine Lines (in cm⁻¹)

J'	F'	0-0 Band R(F'', J')	Δν^a	P(F'', J')	Δν^a	0-1 Band R(F'', J')	Δν^a	P(F'', J')	Δν^a
4.5	2	18 669.282	0.107 (22)[b]			17 837.634	0.092 (8)[b]		
	3	669.175	0.095 (-24)			837.542	0.107 (-12)		
	4	669.080	0.152 (-2)			837.435	0.154 (0)		
	5	668.928	0.189 (-2)			837.281	0.190 (-1)		
	6	668.739	0.231 (2)			837.091	0.231 (2)		
	7	668.508				836.860			
5.5	3	669.803	0.085 (5)	18 661.231	0.075 (7)[b]	838.185	0.102 (23)	17 829.601	0.073 (5)[b]
	4	669.718	0.103 (1)	661.156	0.080 (0)	838.083	0.103 (1)	829.528	0.079 (-1)
	5	669.615	0.125 (0)	661.076	0.088 (-3)	837.980	0.124 (-1)	829.449	0.091 (-1)
	6	669.490	0.148 (0)	660.987	0.102 (-1)	837.856	0.147 (0)	829.358	0.100 (-3)
	7	669.342	0.167 (-3)	660.885	0.109 (5)	837.709	0.167 (-3)	829.258	0.109 (-5)
	8	669.175		660.776		837.542		829.149	
6.5	4	670.320	0.072 (-1)	660.378	0.065 (3)	838.706	0.073 (0)	828.766	0.062 (0)
	5	670.248	0.089 (0)	660.313	0.072 (1)	838.633	0.089 (1)	828.704	0.073 (2)
	6	670.159	0.104 (0)	660.241	0.081 (1)	838.544	0.104 (0)	828.631	0.079 (-1)
	7	670.055	0.118 (-2)	660.160	0.087 (-2)	838.440	0.117 (-2)	828.552	0.087 (-2)
	8	669.937	0.134 (-1)	660.073	0.093 (-5)	838.323	0.138 (4)	828.465	0.093 (-5)
	9	669.803		659.980		838.185		828.372	
7.5	5	670.848	0.067 (1)	659.505	0.053 (-3)	839.253	0.065 (-1)	827.913	0.057 (1)
	6	670.781	0.077 (-1)	659.452	0.065 (1)	839.188	0.075 (-2)	827.856	0.062 (-1)
	7	670.704	0.088 (-1)	659.387	0.070 (-1)	839.113	0.091 (-2)	827.798	0.071 (0)
	8	670.616	0.100 (0)	659.317	0.080 (2)	839.022	0.098 (-2)	827.647	0.076 (-2)
	9	670.516	0.110 (-1)	659.237	0.082 (-3)	838.924	0.108 (-3)	827.647	0.081 (-4)
	10	670.406		659.155		838.816		827.566	
8.5	6	671.361	0.059 (-1)	658.622	0.051 (0)	839.798	0.059 (-1)	827.057	0.053 (2)
	7	671.302	0.068 (-1)	658.571	0.056 (-1)	839.739	0.067 (-2)	827.004	0.057 (0)
	8	671.234	0.077 (0)	658.515	0.061 (-2)	839.672	0.078 (1)	826.947	0.062 (-1)
	9	671.157	0.085 (-1)	658.454	0.070 (1)	839.594	0.085 (0)	826.885	0.067 (-2)
	10	671.072	0.092 (-2)	658.384	0.071 (-3)	839.509	0.092 (-2)	826.818	0.072 (-2)
	11	670.980		658.313		839.417		826.746	

Table 2B (continued)

J"	F"	0-0 Band				0-1 Band			
		R(F", J")	Δν^a	P(F", J")	Δν^a	R(F", J")	Δν^a	P(F", J")	Δν^a
9.5	7	18 671.866	0.053 (-1)	18 657.725	0.075 (28)	17 840.331	0.053 (-1)	17 826.211	0.046 (-1)
	8	671.813	0.061 (0)	657.650	0.021 (-31)	840.278	0.061 (0)	826.140	0.053 (1)
	9	671.752	0.067 (-1)	657.629	0.058 (1)	840.217	0.068 (0)	826.087	0.056 (-1)
	10	671.685	0.075 (1)	657.571	0.061 (0)	840.149	0.073 (-1)	826.031	0.060 (-1)
	11	671.610	0.079 (-2)	657.510	0.063 (-3)	840.076	0.080 (-1)	825.971	0.063 (-3)
	12	671.531		657.447		839.996		825.908	
10.5	8	672.369	0.050 (0)	656.814	0.041 (-2)	840.854	0.053 (3)	825.304	0.044 (1)
	9	672.319	0.054 (-1)	656.773	0.047 (0)	840.801	0.051 (-4)	825.260	0.047 (0)
	10	672.265	0.060 (0)	656.726	0.051 (0)	840.750	0.059 (-1)	825.213	0.050 (-1)
	11	672.205	0.065 (-1)	656.675	0.056 (1)	840.691	0.065 (-1)	825.163	0.053 (-2)
	12	672.140	0.070 (-1)	656.619	0.056 (-3)	840.626	0.071 (0)	825.110	0.056 (-3)
	13	672.070		656.563		840.555		825.054	
11.5	9	672.847	0.044 (-1)	655.888	0.038 (-1)	841.365	0.044 (-1)	824.407	0.040 (0)
	10	672.803	0.048 (-2)	655.850	0.045 (2)	841.321	0.048 (-2)	824.367	0.043 (0)
	11	672.755	0.054 (0)	655.805	0.045 (-1)	841.273	0.054 (0)	824.324	0.044 (-2)
	12	672.701	0.060 (2)	655.760	0.049 (0)	841.219	0.057 (-1)	824.280	0.050 (0)
	13	672.641	0.062 (0)	655.711	0.052 (-1)	841.162	0.064 (2)	824.230	0.051 (-2)
	14	672.579		655.659		841.098		824.179	
12.5	10	673.310	0.041 (-1)	654.942	0.034 (-3)	841.865	0.038 (-4)	823.500	0.039 (2)
	11	673.269	0.045 (0)	654.908	0.041 (2)	841.827	0.046 (1)	823.461	0.038 (-1)
	12	673.224	0.049 (0)	654.867	0.042 (0)	841.781	0.049 (0)	823.423	0.040 (-2)
	13	673.175	0.052 (0)	654.825	0.044 (-1)	841.732	0.051 (-1)	823.383	0.045 (0)
	14	673.123	0.055 (-1)	654.781	0.048 (0)	841.681	0.056 (0)	823.338	0.047 (-1)
	15	673.068		654.733		841.625		823.291	
13.5	11	673.754	0.037 (-1)	653.979	0.032 (-2)	842.347	0.037 (-1)	822.573	0.051 (-3)
	12	673.717	0.041 (0)	653.947	0.036 (0)	842.310	0.042 (1)	822.542	0.056 (0)
	13	673.676	0.045 (1)	653.911	0.039 (0)	842.268	0.045 (1)	822.506	0.039 (0)
	14	673.631	0.045 (-2)	653.872	0.041 (0)	842.223	0.046 (-1)	822.467	0.038 (-3)
	15	673.585	0.049 (-1)	653.831	0.041 (-2)	842.177	0.049 (-1)	822.429	0.041 (-2)
	16	673.538		653.790		842.128		822.388	

Table 2B (concluded)

		0-0 Band				0-1 Band			
J'	F'	R(F'', J'')	$\Delta\nu^a$	P(F'', J'')	$\Delta\nu^a$	R(F'', J'')	$\Delta\nu^a$	P(F'', J'')	$\Delta\nu^a$
14.5	12	18 674.184	0.036 (1)	18 652.999	0.029 (-2)	17 842.817	0.034 (-1)	17 821.633	0.032 (1)
	13	674.148	0.036 (-2)	652.970	0.032 (-1)	842.783	0.037 (-1)	821.611	0.032 (-1)
	14	674.112	0.041 (1)	652.938	0.036 (1)	842.746	0.041 (1)	821.569	0.035 (0)
	15	674.071	0.042 (-1)	652.902	0.038 (1)	842.705	0.042 (-1)	821.534	0.037 (0)
	16	674.029	0.044 (-1)	652.864	0.037 (-2)	842.663	0.046 (1)	821.497	0.037 (0)
	17	673.985		652.827		842.617		821.460	0.037 (-2)
15.5	13	674.599	0.030 (-3)					820.680	0.027 (-2)
	14	674.569	0.035 (0)					820.653	0.029 (-2)
	15	674.534	0.037 (0)					820.624	0.033 (1)
	16	674.497	0.040 (1)					820.591	0.034 (0)
	17	674.457	0.038 (-3)					820.557	0.033 (-3)
	18	674.419						820.524	
16.5	14	674.992	0.026 (-4)						
	15	674.966	0.032 (0)						
	16	674.934	0.033 (-1)						
	17	674.901	0.037 (2)						
	18	674.864	0.036 (-1)						
	19	674.828							

[a]For each hyperfine multiplet, the 5 tabulated differences between adjacent components were input to the hyperfine fit.

[b]Observed minus calculated, in 10^{-3} cm^{-1}.

Table 2C. Intercombination: Upper State System XVII - Lower State System XXI

0-0 Band Hyperfine Lines (in cm^{-1})

J'	F"	R(F', J")	$\Delta\nu^a$		P(F', J")	$\Delta\nu^a$	
4.5	2	16 380.977	0.088	(6)[b]			
	3	380.889	0.111	(-5)			
	4	380.778	0.150	(-1)			
	5	380.628	0.187	(0)			
	6	380.441	0.226	(2)			
	7	380.215					
5.5	3	381.498	0.076	(-1)	16 372.907	0.067	(-1)[b]
	4	381.422	0.100	(0)	372.840	0.076	(-1)
	5	381.322	0.122	(0)	372.764	0.085	(-2)
	6	381.200	0.143	(-1)	372.679	0.096	(-2)
	7	381.057	0.165	(-1)	372.583	0.103	(-5)
	8	380.892			372.480		
6.5	4	382.035	0.070	(-1)	372.061	0.061	(2)
	5	381.965	0.086	(0)	372.000	0.068	(0)
	6	381.879	0.102	(0)	371.932	0.076	(-1)
	7	381.777	0.115	(-2)	371.856	0.082	(-3)
	8	381.662	0.131	(-1)	371.774	0.090	(-3)
	9	381.531			371.684		
7.5	5	382.592	0.065	(1)	371.203	0.054	(0)
	6	382.507	0.074	(-2)	371.149	0.062	(1)
	7	382.433	0.086	(-1)	371.087	0.067	(-1)
	8	382.347	0.097	(-1)	371.020	0.073	(-2)
	9	382.250	0.107	(-1)	370.947	0.078	(3)
	10	382.143			370.869		
8.5	6	383.104	0.058	(0)			
	7	383.046	0.066	(-1)			
	8	382.980	0.076	(0)			
	9	382.904	0.082	(-2)			
	10	382.822	0.091	(-1)			
	11	382.731					
9.5	7	383.627	0.053	(0)	369.446	0.046	(1)
	8	383.579	0.059	(-1)	369.400	0.049	(-1)
	9	383.515	0.066	(-1)	369.351	0.054	(-1)
	10	383.449	0.072	(-1)	369.297	0.058	(-1)
	11	383.377	0.081	(2)	369.239	0.059	(-4)
	12	383.296			369.180		

Table 2C (continued)

J"	F'	R(F'', J'')	$\Delta\nu^a$		P(F'', J'')	$\Delta\nu^a$	
10.5	8	16 384.135	0.048	(-1)	16 368.546	0.042	(0)
	9	384.087	0.059	(0)	368.504	0.045	(-1)
	10	384.033	0.058	(-1)	368.459	0.049	(0)
	11	383.975	0.065	(1)	368.410	0.052	(-1)
	12	383.910	0.067	(-2)	368.358	0.054	(-3)
	13	383.843			368.304		
11.5	9	384.629	0.044	(-1)	367.634	0.039	(0)
	10	384.585	0.049	(0)	367.595	0.042	(0)
	11	384.536	0.052	(1)	367.533	0.044	(-1)
	12	384.484	0.057	(0)	367.509	0.047	(-1)
	13	384.427	0.060	(-1)	367.462	0.049	(-2)
	14	384.367			367.413		
12.5	10	385.112	0.040	(-1)	366.705	0.035	(-1)
	11	385.072	0.045	(0)	366.670	0.038	(0)
	12	385.027	0.047	(-1)	366.632	0.040	(-1)
	13	384.980	0.050	(-2)	366.592	0.043	(-1)
	14	384.930	0.054	(-1)	366.549	0.045	(-1)
	15	384.876			366.504		
13.5	11	385.578	0.037	(-1)	365.762	0.033	(0)
	12	385.541	0.041	(0)	365.729	0.035	(0)
	13	385.500	0.043	(-1)	365.694	0.037	(-1)
	14	385.457	0.046	(-1)	365.657	0.040	(0)
	15	385.411	0.049	(0)	365.617	0.040	(-2)
	16	385.362			365.577		
14.5	12	386.030	0.034	(-1)	365.806	0.030	(-1)
	13	386.996	0.038	(0)	364.776	0.032	(-1)
	14	386.968	0.040	(0)	364.744	0.034	(-1)
	15	385.918	0.042	(0)	364.710	0.037	(0)
	16	385.876	0.048	(3)	364.673	0.037	(-1)
	17	385.828			364.636		
15.5	13	386.464	0.032	(0)	363.830	0.027	(-1)
	14	386.432	0.035	(0)	363.803	0.030	(0)
	15	386.397	0.036	(-2)	363.773	0.032	(0)
	16	386.361	0.038	(-1)	363.741	0.034	(-2)
	17	386.323	0.040	(-1)	363.707	0.033	(-2)
	18	386.283			363.674		
16.5	14	386.885	0.030	(0)	362.838	0.024	(-2)
	15	386.855	0.031	(-1)	362.814	0.028	(0)
	16	386.824	0.034	(0)	362.786	0.030	(1)
	17	386.790	0.037	(1)	362.756	0.031	(0)
	18	386.753	0.035	(-2)	362.725	0.031	(-1)
	19	386.718			362.694		

Table 2C (concluded)

J'	F'	R(F', J')	$\Delta_\nu{}^a$		P(F'', J'')	$\Delta_\nu{}^a$	
17.5	15	16 387.287			16 361.829		
	16	387.260	0.027	(-1)	361.809	0.020	(-4)
	17	387.230	0.030	(0)	361.780	0.029	(3)
	18	387.199	0.031	(0)	361.754	0.026	(-1)
	19	387.166	0.033	(0)	361.726	0.028	(0)
	20	387.132	0.034	(0)	361.698	0.028	(-2)
18.5	16	387.673			360.808		
	17	387.648	0.025	(-1)	360.786	0.022	(-1)
	18	387.619	0.029	(2)	360.761	0.025	(1)
	19	387.591	0.028	(0)	360.737	0.024	(-1)
	20	387.559	0.032	(2)	360.710	0.027	(1)
	21	387.528	0.031	(0)	360.683	0.07	(0)
19.5	17	388.039					
	18	388.017	0.022	(-2)			
	19	387.991	0.026	(1)			
	20	387.962	0.029	(2)			
	21	387.932	0.030	(2)			
	22	387.902	0.030	(1)			

[a] For each hyperfine multiplet, the 5 tabulated differences between adjacent components were input to the hyperfine fit.

[b] Observed minus calculated, in 10^{-3} cm^{-1}.

Table 3. XVII and XXI System Molecular Constants

State Ω	T_v(cm^{-1})	B_v(cm^{-1})	D_v(cm^{-1}) $\times$ 10^7	d(cm^{-1})	d_j $\times$ 10^4(cm^{-1})
4.5	18 882.388 (2)	0.353001 (18)	2.87 (24)	0.12403 (71)	1.031 (54)
4.5	16 594.075 (1)	0.353736 (20)	4.79 (30)	0.12977 (67)	1.216 (35)
4.5 (v=1)	1 049.035 (2)[a]	0.360719 (21)	3.41 (31)	0.27691 (80)	2.011 (72)
4.5 (v=0)	217.383 (1)	0.362134 (20)	3.38 (28)	0.27744 (66)	2.042 (47)
3.5	0.0	0.360948 (16)	3.22 (15)	-0.00809 (85)	-

1σ uncertainties in parentheses

[a]$\Delta G_{1/2}$ = 831.652 (2)

Table 4.   Molecular Constants for Low-Lying States Observed
           Through Fluorescence from the XXI and XVII Systems

STATE Ω	$T_0(cm^{-1})$	$B_0(cm^{-1})$	$D_0(cm^{-1}) \times 10^7$
4.5	18 882.388 (2)	0.353001 (18)	2.87 (24)
4.5	16 594.075 (1)	0.353736 (20)	4.79 (30)
3.5	3 887.15 (16)[b]	0.35751 (28)	3.30[a]
3.5	2 931.66 (15)	0.35712 (21)	3.30[a]
4.5	2 155.16 (30)	0.36264 (67)	3.30[a]
3.5	2 099.16 (31)	0.35879 (71)	3.30[a]
3.5	2 064.34 (13)[c]	0.35654 (20)	3.30[a]
4.5	217.383 (1)[d]	0.362134 (20)	3.30 (28)
3.5	0.0	0.360948 (16)	3.22 (15)

1σ uncertainties in parentheses

[a]Fixed to D_0 from the lower state of the XVII System ($\Omega" = 3.5$)

[b]$\Delta G_{1/2} = 831.73$ (51)

[c]$\Delta G_{1/2} = 826.47$ (21)

[d]$\Delta G_{1/2} = 831.652$ (2)

Optical Optical Double Resonance Spectra
of Cerium Oxide

C. LINTON

Physics Department
University of New Brunswick
Fredericton, New Brunswick
Canada   E3B 5A3

and

M. DULICK
Department of Chemistry
and Spectroscopy Laboratory
Massachusetts Institute of Technology
Cambridge, Massachusetts 02139, U.S.A.

7   Pages Manuscript

1   Page Tables

1   Page Figure Captions

2   Pages Figures

In a recent publication (1), results of some laser-induced fluorescence experiments on CeO were outlined. From these results, it was possible to determine the relative energies of seven low lying electronic states and include them all on one energy level diagram. Further experiments have led to the addition of nine low lying states to this level diagram (results reported at a recent meeting (2), details to be published shortly).

In addition to fluorescence experiments, optical optical double resonance (OODR) experiments have been performed in which CeO molecules were excited sequentially with radiation from CW argon ion and CW dye (with Rhodamine 6G) lasers. The molecules were formed in a Broida oven (3,4) in which CeO was made by reacting Ce vapor with O_2 or CO_2. The total pressure (mainly Argon, which was used as a carrier gas) was 4-5 Torr. The argon laser pumped a known transition and fluorescence from the pumped excited state was monitored at a given wavelength through a monochromator. The dye laser was scanned (multimode) and its excitation spectrum, which was detected using a suitable filter plus photomultiplier combination, was recorded while simultaneously monitoring the OODR excitation spectrum as changes in resolved argon laser fluorescence intensity. The spectra were calibrated by passing a portion of the beam through an etalon and recording the etalon fringes together with the excitation spectrum on a two pen recorder. The free spectral range of the etalon was 3.054 ± 0.01 cm^{-1}. To get an absolute wavelength calibration, the positions at which fluorescence from the sodium D lines occurred were noted on the chart.

It was observed that when resolved argon laser excited fluorescence was monitored with a monochromator while the dye laser was scanned, several bands in the excitation spectrum would be accompanied by large decreases in the argon fluorescence intensity while other bands would be accompanied by increases. Because of the high pressure (~5 Torr) at which these experiments were performed, relaxation between states was very probable, especially between long-lived close-lying states. Decreases in argon fluorescence should occur when the dye laser transition involves the same lower state as the argon laser transition. The dye laser would thus deplete the population of the lower state, with the result that the argon laser can pump fewer molecules to the upper state and the fluorescence decreases. This would also occur if the lower levels were not identical, but close enough in energy to be collisionally connected. Several argon laser transitions were investigated: two $C_1(\Omega=3)-X_1(\Omega=2)$ transitions pumped by the 514.53 nm line, the $g_2(2)-X_2(3)$ transition pumped by the 476.49 nm line, and the $D_3(5)-X_3(4)$ transition pumped by the 487.99 nm line.

The 514.53 nm line of the argon laser pumps two transitions, $P(25)$ 0-1 and $R(29)$ 1-2 in the $C_1(3)-X_1(2)$ system (4). In the first experiment, the argon laser, operating single mode, was tuned to pump $P(25)$ 0-1 and the monochromator was tuned to detect $Q(24)$ 0-0 at 493.2 nm. The spectrum, portions of which are shown in Fig. 1, shows several large decreases (~20%) in the intensity of the monitored fluorescence and a few increases. Many of the bands in the excitation spectrum to which these decreases correspond have not been assigned. However, decreases were observed

when the dye laser excited transitions which have been shown from fluorescence data to be $B_1(2)-X_1(2)$ 1-1, $E_2(4)-X_2(3)$ 1-1 and $e_2(3)-X_2(3)$ 1-1. In addition, a decrease was observed at ~583.5 nm, which is the position calculated for the $e_2(3)-X_1(2)$ 1-1 band based on the observation from fluorescence data (1) that $X_2(3)$ is 80 cm^{-1} above $X_1(2)$. All assigned transitions in the Rhodamine 6G region involving $X_1(2)$, v=1 and $X_2(3)$, v=1 give decreases in the monitored fluorescence. As the argon laser is pumping from $X_1(2)$, v=1, decreases are then expected for all transitions involving this state. The additional large decreases for $X_2(3)$, v=1 indicate that collisional relaxation between the $X_1(2)$, v=1 and $X_2(3)$, v=1 states is very efficient and are consistent with the states being close in energy. The banded nature of the decreases shows that the spectra were rotationally relaxed. However, the absence of decreases at other vibrational levels of $X_1(2)$ or $X_2(3)$ indicates that vibrational relaxation is not significant. The spectra thus confirm previous assignments of 1-1 bands. The efficient relaxation, together with assignment of $e_2(3)-X_1(2)$ 1-1, confirm the calculated separation (1) of the $X_1(2)$ and $X_2(3)$ states. Fig. 2 is an energy level diagram which summarizes these double resonances.

Other argon laser transitions were not investigated as thoroughly as the above. In each case, just one survey spectrum was obtained with the argon laser in multimode operation. Double resonances involving the $C_1(3)-X_1(2)$ 1-2 transition pumped by the 514.53 nm line were observed by monitoring Q(30) 1-1 at 494.2 nm. Decreases in the argon laser induced fluorescence occurred at

calculated positions of the 2-2 bands of the $B_1(2)-X_1(2)$, $e_2(3)-X_2(3)$ and $E_2(4)-X_2(3)$ transitions, but not at wavelengths corresponding to transitions which involve any other vibrational levels of the $X_1(2)$ and $X_2(3)$ states. This again illustrates the efficiency of the collisional relaxation between the adjacent $X_1(2)$ and $X_2(3)$ states.

With the argon laser at 476.49 nm pumping $g_2(2)-X_2(3)$ 0-0 Q(30) and the monochromator monitoring R(29), decreases were observed in the $B_1(2)-X_1(2)$ 0-0 and $e_2(3)-X_2(3)$ 0-0 transitions. These are also consistent with the above mechanism. The signal to noise ratio in this spectrum was very poor so that other decreases probably were not detected.

The 487.99 nm line of the argon laser excited the P(37) line of $D_3(5)-X_3(4)$ 0-0 (4,5). With the monochromator set to monitor Q(36), a sharp decrease was observed when the dye laser pumped $C_3(4)-X_3(4)$ 0-0. Another strong decrease was observed at the calculated position of $C_3(4)-X_3(4)$ 1-0. This band head lies within 2 cm^{-1} of the strong $e_2(3)-X_2(3)$ 0-0 band and had not been detected in absorption or emission spectra. A complete list of assigned transitions responsible for decreases in fluorescence is given in table I.

In each of the double resonance experiments described above, several decreases, some quite strong, could not be connected with known transitions. As all decreases that could be assigned are consistent with the same mechanism, it is probable that the transitions responsible for the unassigned decreases involve the lower state of the transition excited by the argon laser, or one that is

close enough in energy that collisional transfer is efficient. In some cases, this could mean a choice between several candidates. For example, $X_2(3)$ v=1, u(2) v=0, and y(1) v=0 (2) all are within 100 cm^{-1} of $X_1(2)$ v=1.

In addition to the decreases mentioned above, there were many dye laser excited transitions that increased the intensity .of the monitored fluorescence transition. One possible mechanism would be that the lower state of the transition pumped by the argon laser is being radiatively populated from the upper state of the transition excited by the dye laser. There are several assigned examples of this effect. When the 514.53 nm Ar$^+$ line pumped the $C_1(3)-X_1(2)$ 0-1 band, a strong increase in fluorescence was observed when the dye laser pumped $B_1(2)-X_1(2)$ 0-0. This could have been caused by an increase in the population of $X_1(2)$ v=1 via the $B_1(2)-X_1(2)$ 0-1 transition which was observed to be quite intense in fluorescence spectra. Excitation of $e_2(3)-X_2(3)$ 0-0 caused a very sharp increase in $D_3(5)-X_3(4)$ 0-0 fluorescence. The $e_2(3)-X_3(4)$ transition which would account for the increase in the population of $X_3(4)$ was prominent in fluorescence when $e_2(3)-X_2(3)$ was excited. There were many more OODR increases. All cases involving known transitions could be explained by the above model and, in most cases, the transition responsible for increasing the lower state population was observed to be strong in fluorescence spectra.

The double resonance experiments described above all lead to the same consistent interpretation of the observed decreases and increases in monitored fluorescence intensity. While the increases were not particularly useful here, the results highlight the value

of the decreases. Many diatomic molecules, especially those
involving heavy atoms, have numerous low lying states which
often are difficult to link in a single energy level diagram.
Because the radiative transition probability is proportional to
ν^3, these states are necessarily long-lived and collisional
redistribution is inevitable. The OODR decreases have enabled
us to determine which of these states are close in energy and to
identify heads of vibrationally excited bands which in absorption
and emission spectra, either do not appear or are obscured by
intense overlapping bands. The energy separation, ΔE, has been
shown to be a critical factor in determining the probability
of efficient collisional transfer between two states. The
relative importance of other factors, such as Δv or $\Delta \Omega$, could be
determined if all the OODR decreases could be assigned. The OODR
technique may also be useful in identifying those transitions
sharing a common lower state, but such experiments would require
lower pressures to minimize collisional transfer.

Acknowledgments

REFERENCES

1. C. LINTON, M. DULICK, R.W. FIELD, P. CARETTE and R.F. BARROW, J. Chem. Phys. 73, (1980).

2. C. LINTON, M. DULICK and R.W. FIELD, Divisional Meeting of Atomic and Molecular Physics Division, Canadian Association of Physicists (1980).

3. J.B. WEST, R.S. BRADFORD, JR., J.D. EVERSOLE, and C.R. JONES, Rev. Sci. Instrum. 46, 164-168 (1975).

4. C. LINTON, M. DULICK and R.W. FIELD, J. Mol. Spectrosc. 78, 428-436 (1979).

5. R.F. BARROW, R.M. CLEMENTS, S.M. HARRIS and P.P. JENSON, Astrophys. J., 229, 439-447 (1979).

TABLE I: ASSIGNMENTS OF DYE LASER EXCITED TRANSITIONS IN CeO CAUSING DECREASES IN FLUORESCENCE INTENSITY OF TRANSITIONS PUMPED BY AN ARGON LASER.

Wavelength (nm)	Wavenumber (cm^{-1})	Assignment
A. Pumped Transition $C_1(3)$-$X_1(2)$ 0-1; Wavelength 514.53 nm		
583.54[a,c]	17 132.1	$e_2(3)$-$X_1(2)$ 1-1
586.35[b,c]	17 049.9	$e_2(3)$-$X_2(3)$ 1-1
608.39[b,c]	16 432.3	$B_1(2)$-$X_1(2)$ 1-1
611.59[b,c]	16 346.3	$E_2(4)$-$X_2(3)$ 1-1
B. Pumped Transition $C_1(3)$-$X_1(2)$ 1-2; Wavelength 514.53 nm		
588.19[a,c]	16 996.5	$e_2(3)$-$X_2(3)$ 2-2
612.30[a,c]	16 327.4	$B_1(2)$-$X_1(2)$ 2-2
614.18[a,c]	16 277.3	$E_2(4)$-$X_2(3)$ 2-2
C. Pumped Transition $g_2(2)$-$X_2(3)$ 0-0; Wavelength 476.49 nm		
584.37[b]	17 107.7	$e_2(3)$-$X_2(3)$ 0-0
604.58[b]	16 535.9	$B_1(2)$-$X_1(2)$ 0-0
D. Pumped Transition $D_3(5)$-$X_3(4)$ 0-0; Wavelength 487.99 nm		
584.31[c]	17 109.5	$C_3(4)$-$X_3(4)$ 1-0
611.19[b]	16 356.9	$C_3(4)$-$X_3(4)$ 0-0

a. Relative accuracy 0.1 nm, 3 cm^{-1}
b. Wavelength from ref. 5
c. New assignment

Figure Captions

Figure 1   Optical optical double resonance spectra of CeO. The $C_1(3)$-$X_1(2)$ 0-1 transition is excited by the 514.53 nm line of an argon laser. The upper spectrum shows the change in 0-0 fluorescence at 493.2 nm as the dye laser is scanned. The dye laser excitation spectrum is shown in the lower trace.

Figure 2   Energy diagram showing transitions responsible for decreases in fluorescence intensity after excitation of the $C_1(3)$-$X_1(2)$ 0-1 transition of CeO.